Applied Geochemistry 200 (2026) 106738

Contents lists available at ScienceDirect

Applied Geochemistry

journal homepage: www.elsevier.com/locate/apgeochem

Spatial variations in groundwater chemistry in Uganda: Geogenic origins and geochemical controls across diverse hydrogeological settings

Derick Muloogi [a,b], George J.L. Wilson [a], Farah T. Ahmed [a,c], David A. Polya [a], Laura A. Richards [a,*]

[a] Department of Earth and Environmental Sciences and Williamson Research Centre for Molecular Environmental Science, The University of Manchester, Williamson Building, Oxford Road, Manchester, M13 9PL, United Kingdom
[b] Department of Energy, Minerals, and Petroleum Studies, Mbarara University of Science and Technology, P.O Box 1410, Mbarara, Uganda
[c] Bangladesh Atomic Energy Commission, Paramanu Bhaban, Agargaon, Dhaka, 1207, Bangladesh

ARTICLE INFO

Editorial handling by: Elisa Sacchi

Keywords:
Groundwater
Hydrogeological settings
East Africa
Silicate and carbonate weathering
Cation exchange

ABSTRACT

Groundwater sustains about 75 % of Uganda's population, particularly in rural and peri-urban areas. However, the baseline hydrogeochemistry of operational community water sources remains poorly understood. Using hydrochemical analysis and geochemical modelling, we assessed groundwater inorganic geochemistry and geochemical controls across five distinct hydrogeological settings in Uganda: Precambrian metasedimentary (MS; $n = 30$), granulitic-gneissic complex (GG; $n = 21$), unconsolidated sedimentary (SDM; $n = 10$), volcanics (VO; $n = 7$), and metavolcanics (MV; $n = 6$). Results show that Ca–HCO_3 is the predominant hydrochemical facies in most settings, reflecting limited geochemical evolution, whereas Na–HCO_3 and Na–Cl facies dominate MV and SDM, consistent with cation exchange and advanced geochemical evolution. World Health Organisation (WHO) drinking water guidelines for selected targets were exceeded in 3 % of samples (for Fe, F^-, and Cl^-), 5 % for Mn, and 14 % for NO_3^-. By settings, exceedances were: (i) MS – 20 % NO_3^-, 13 % Mn, and 7 % Cl^-; (ii) GG – 14 % NO_3^-, and 5 % Fe; (iii) MV –17 % Fe; and (iv) SDM – 10 % F^-, indicating more frequent guideline exceedances in MS. Major-ion ratios, including $(Na^+ + K^+)/Cl^-$ ratios (> 1), HCO_3^-/Na^+ (1–4), $(Ca^{2+} + Mg^{2+})/HCO_3^-$ (~0.3–0.8), and $(Ca^{2+} + Mg^{2+})/SO_4^{2-}$ (>1), are consistent with active silicate weathering, cation exchange, and contributions from carbonate dissolution, with minimal influence from evaporative concentration and gypsum dissolution. Geochemical modelling shows undersaturation for calcite, dolomite, and gypsum, but quartz supersaturation. Thermodynamic modelling indicates kaolinite as the stable secondary mineral in VO, contrasting clinoptilolite in other settings, reflecting active monosiallitisation under rapid flow, well-drained conditions, and low silica accumulation. This study establishes baseline hydrogeochemical characterisation across Uganda's diverse hydrogeologies, highlighting spatial variability and controls to inform targeted, sustainable groundwater management.

1. Introduction

At the heart of East Africa lies Uganda, a landlocked country renowned for its extensive surface waters, including Lake Victoria and the River Nile. However, groundwater – a vital yet lesser-understood resource – supports approximately 75 % of the population (MWE, 2024; Nsubuga et al., 2014; Tindimugaya, 2005) for domestic purposes, especially in rural and peri-urban areas. With the second-youngest population globally (UNICEF Uganda, 2024), Uganda's growing demographic is driving an increase in groundwater demand. Although often perceived as safer than surface water, the presence of chemical and microbial contaminants in groundwater has been reported (Howard et al., 2003; Wilson et al., 2024a; Uzorka et al., 2025), and pollutant hazards are amplified by the limited availability of treated, piped drinking water across the country (NWSC, 2023; Okot-Okumu and Otim, 2015). Growing reliance on groundwater, coupled with its potential susceptibility to surface-derived pollutant ingress through natural or anthropogenically-influenced processes (Owor et al., 2011; Wilson et al., 2024a), highlights the need to understand how (hydro)geology influences water quality and chemistry across contrasting hydrogeological

* Corresponding author.
E-mail address: laura.richards@manchester.ac.uk (L.A. Richards).

https://doi.org/10.1016/j.apgeochem.2026.106738
Received 7 October 2025; Received in revised form 18 February 2026; Accepted 19 February 2026
Available online 24 February 2026
0883-2927/© 2026 The Authors. Published by Elsevier Ltd. This is an open access article under the CC BY license (http://creativecommons.org/licenses/by/4.0/).

settings in Uganda. Such understanding is particularly important, as efforts towards safe drinking water provision in Uganda are still challenged by limited access to robust baseline water quality data (MWE, 2017; Richards et al., 2023).

Uganda's hydrogeology is varied and characterised by different rock types and tectono-thermal properties (Schlüter, 2008; Westerhof et al., 2014). The geological units include ancient granulitic gneisses, meta-sedimentary rocks, volcanic rocks, cataclasites, granite intrusions, metamorphic rocks, meta-igneous rocks, and unconsolidated sediments (BGS, 2019; Westerhof et al., 2014). Distributed across different regions, these units represent geological periods ranging from the Neo-Archaean to the Miocene (Westerhof et al., 2014). This contrast in geological environments contributes to distinct groundwater systems that are governed by complex geochemical processes, resulting in variability in groundwater chemistry (Drever, 1988; Elango and Kannan, 2007; Owor et al., 2021; Walraevens et al., 2018).

The hydrogeologic properties of rocks strongly influence the extent of water-rock interactions. Relatively high groundwater flow velocities typically result in groundwater with relatively low dissolved solids, due to shorter rock contact times and higher water-to-rock ratios, and vice versa (Langmuir, 1997). Additionally, the mineralogical composition of aquifers plays a crucial role in determining water chemistry (Jebreen et al., 2018; Njitchoua et al., 1997; Pincetti-Zúniga et al., 2020). Fast-dissolving minerals like metal carbonates markedly alter the water chemistry, while slower-dissolving silicates contribute more subtly except where there is longer term water-rock interaction (Mackenzie and Garrels, 1965, 1971). Further, local aquifer depths influence groundwater composition, with anions in shallow waters typically being bicarbonate-dominated (HCO_3^-) due to silicate and carbonate weathering, although in some shallow settings, sulphates (SO_4^{2-}) and chloride (Cl^-) can become relatively enriched due to stronger evaporation (Agbasi et al., 2025).Intermediate depths are often characterised by increased SO_4^{2-}, while deeper waters contain higher Cl^- concentrations, reflecting longer residence times and cumulative rock-water interactions (Chebotarev, 1955). As a result, contrasting groundwater types emerge, each exhibiting unique characteristics influenced by the underlying hydrogeological features.

In Uganda, variable groundwater types have been reported (Owor et al., 2021; Muloogi et al., 2025), and which potentially relate to variations in the distribution of health or operationally-relevant geogenic contaminants, such as fluoride (BGS, 2001; Egor and Birungi, 2020; Ojok et al., 2021), manganese (Lapworth et al., 2020), and iron (Bakyayita et al., 2019; Fader, 2011; Flynn et al., 2012; Taylor and Howard, 1995). In regions where human activities may influence groundwater sources, particularly shallow aquifers, anthropogenic pollutants such as nitrate (NO_3^-), sulphate (SO_4^{2-}), and phosphate (PO_4) have increasingly been reported, often linked to contaminant ingress from agricultural practices, urbanisation, and inadequate sanitation infrastructure (Kulabako et al., 2008; Lapworth et al., 2020; Musumba et al., 2022; Nyenje et al., 2013, 2014; Wilson et al., 2024a).

Groundwater abstraction in Uganda predominantly occurs from relatively cheap-to-access, but vulnerable shallow sources, such as saprolite and saprock, along with some deeper extractions from heterogeneous basement aquifers (Nyenje et al., 2022; Taylor and Howard, 1995). The basement aquifers are composed of crystalline rocks with varying origins and compositions across distinct hydrogeological settings (MWE, 2017), underlining the importance of understanding the processes controlling groundwater geochemistry. Localised studies in Uganda have examined groundwater-lithology interactions (Guma et al., 2021; Kulabako et al., 2007; Nyakairu et al., 2023; Uzorka et al., 2025). In addition, Owor et al. (2021) conducted a national-scale assessment of shallow groundwater quality, but this evaluation was based on samples collected at the time of drilling. Such initial samples may be influenced by drilling fluid contamination (Richards et al., 2015), limiting their reliability for understanding natural geochemical conditions or subsequent water–rock interactions. Consequently, key processes, including post-drilling geochemical evolution, mineral thermodynamic equilibria, and the hydrogeochemical controls in operational community water sources across contrasting hydrogeologies remain largely unknown. These knowledge gaps are further exacerbated in Uganda by the growing pressures from population growth, agricultural expansion, urbanisation (UBOS, 2024), and the long-term cumulative effects of groundwater-rock interactions. Bridging these gaps is essential for effective groundwater management, advancing Sustainable Development Goal 6.1 (United Nations, 2023), and supporting the country's Strategic Investment Plan for the Water and Environment Sector (2018-2030; MWE, 2018).

Here, we assess the spatial variations in groundwater hydrogeochemistry across contrasting hydrogeological settings in Uganda. Our focus is on identifying the geogenic origins, geochemical processes, and controls of groundwater chemistry from communities' domestic and drinking water sources across five of the country's distinct hydrogeological settings. The specific objectives of the study are to: (i) characterise the inorganic geochemistry of groundwater from various sources across Uganda's contrasting hydrogeological formations; (ii) assess the spatial variability in the suitability of groundwater for uses such as drinking and irrigation; iii) delineate the geogenic sources of groundwater contaminants; and (iv) identify the dominant geochemical processes and mechanisms driving the spatial variations in groundwater chemistry.

2. Methodology

2.1. Study area

Uganda, with a total land area of ~241,000 km^2 (BGS, 2001), includes ~ 36,000 km^2 of lakes, notably Lake Victoria along the southeastern border. The country is also the source of the Nile River, which flows 6600 km northwards from Lake Victoria toward the Mediterranean Sea (National Geographic Society, 2023). Most of the sampling was conducted in central and eastern Uganda within the two hydrologically interconnected Lake Victoria and Lake Kyoga basins, including areas extending towards northeastern parts of Mt. Elgon (Fig. 1).

Uganda is predominantly a rural country, with an economy heavily dependent on agriculture. Approximately 43 % of land is arable, pasture, and permanent crops, while only 10 % of the total land area is forested (MWE, 2019). Although only 1 % of farmers countrywide practice irrigation, 55 % of these farmers are concentrated in the eastern region (Mwaura and Muwanika, 2018), where this study primarily focused. Fertiliser use is low at 1–2.5 kg per hectare annually, which is below sub-Saharan Africa's average of 8 kg (MAAIF, 2016). However, fertiliser consumption increased from 41,500 metric tons in 2014 to 66,384 metric tons in 2017 (IFDC and AFAP, 2018). NPK (17:17:17; IFDC and AFAP, 2018) is the most commonly used fertiliser, especially in sugarcane plantations, which are widely cultivated in the study area.

The country's climate is generally tropical, tending towards a semi-arid environment in the north-eastern regions. Rainfall shows marked temporal and spatial variability, with two prominent rainfall regimes (UNMA, 2023). The regions closer to the equator, including those sampled in this study, experience a bimodal regime, with a major rainy season from March to May and a minor (shorter) season from September to December. In contrast, areas farther from the equator have a unimodal rainfall regime, prevailing from June to August (UNMA, 2023). Annual rainfall ranges from over 2000 mm near Lake Victoria and Mt. Elgon to under 700 mm in the northeast. The mean annual temperature is 23.3 °C, with monthly averages between 21.7 °C and 23.9 °C (Kisembe et al., 2019).

2.2. Geology and hydrogeological units of Uganda

Uganda's geology is highly diverse, spanning over three billion years, and shaped by its location in the East African plateau (Westerhof et al.,

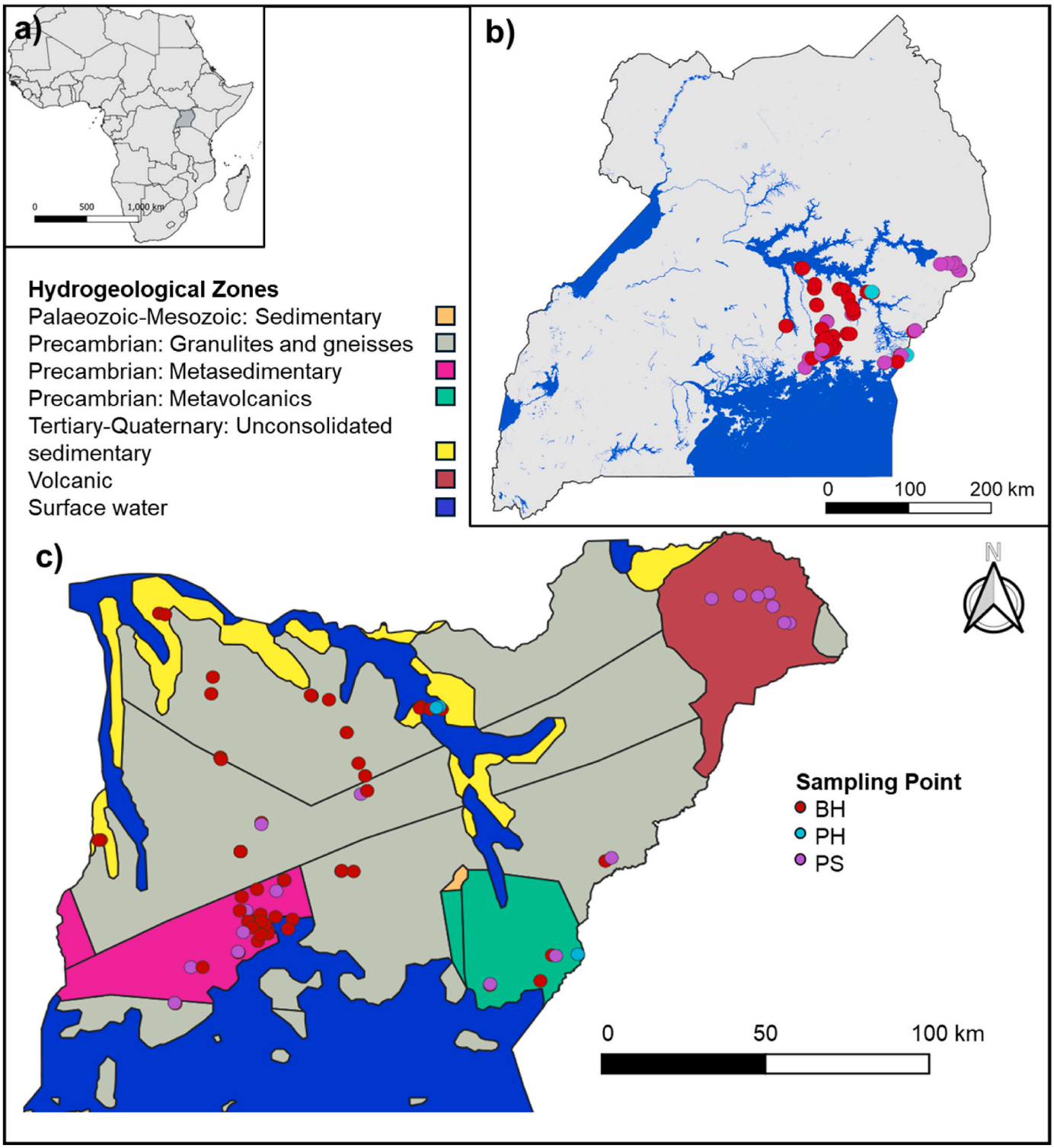

Fig. 1. Maps showing **a)** Uganda's location in Africa, **b)** the sampling sites ($n = 74$), and **c)** the distribution of sites across contrasting hydrogeological settings. The corresponding maps were created based on the following shape files: a - (ICPAC, 2017); b - (OCHA, 2020); and c) - (BGS, 2019). The colour codes represent the different water sources sampled: BH – Borehole, PH – Piped groundwater supply system/Pumps, PS – Protected Spring). The minor apparent mismatches between some GPS points and lithological boundaries reflect limitations in the spatial resolution or generalisation of the national-scale hydrogeological shapefile in comparison to field-obtained location data at sampling sites. (For interpretation of the references to colour in this figure legend, the reader is referred to the Web version of this article.)

2014). The terrain is predominantly underlain by Precambrian crystalline rocks, which constitute most of the country's land area. Approximately 10 % of the terrain is overlain by more recent volcanic and sedimentary rocks (BGS, 2001). The Precambrian basement is covered by a regolith layer, typically around 30 m thick (BGS, 2001). Most groundwater for domestic use is abstracted from this overlying weathered regolith and the fractured bedrock (Nsubuga et al., 2014; Taylor and Howard, 2000). The regolith aquifer is favoured for its promising

yields and lower development costs compared to deeper groundwater from the basement (Taylor and Howard, 2000). Well yields range from 0.5 to 12 $m^3\ h^{-1}$, with higher yields reported in fissured granites and gneisses (Owor et al., 2021), but pervasively low transmissivities across the weathered crystalline-rock aquifers (median $<2\ m^2/d$; Owor et al., 2022). These hydrogeological characteristics are consistent with complex and predominantly localised groundwater flow, reflecting the discontinuous nature of the aquifers and generally short flow paths (Owor et al., 2021).

The prominent geological features of Uganda include the East African Rift along its western border, and the extinct shield volcano (Elgon Complex) in eastern Uganda, straddling the border with Kenya (Westerhof et al., 2014). In central and northern Uganda, the landscape is dominated by ancient metamorphic rocks from the Archaean-Proterozoic era (Westerhof et al., 2014).

This geological diversity not only shapes the country's physical geography, but also provides a framework for the categorisation of its hydrogeological units (BGS, 2019; Cahen et al., 1984; Owor et al., 2021, 2011; Schlüter, 2006; cf. Fig. 1S). This current study focused on key hydrogeological settings, notably those in the eastern and central parts of Uganda:

- Granulitic Gneissic Complex (GG): Widely prevalent, with sampling concentrated in Eastern districts (Iganga, Kaliro, and Tororo).
- Precambrian Metasedimentary Units (MS): Comprised of the Lake Victoria Terrane granite-greenstones, nepheline syenite, and gabbro intrusions, with sampling conducted in Jinja and Buikwe districts.
- Sediments and Unconsolidated Sedimentary Rocks (SDM): Predominant in the southwestern Uganda, particularly in the Karagwe-Ankolean System of the Kibaran Belt, but with great occurrences within the Lake Kyoga Basin. Sampling targeted the Kyoga shoreline districts (Kibuku, Kamuli, Buyende, and Kayunga).
- Volcanics (VO): Featuring the Elgon Complex pyroclastic and lahar-type alkaline/sodic volcanic rocks, as well as carbonatite plugs and fenites, with sampling concentrated in Kween, Bukwo, and Kapchorwa districts.
- Metavolcanics (MV): Comprised of altered volcanic rocks that have undergone metamorphism, found mainly in the eastern and south-eastern regions, with sampling in Busia.

Other (hydro)geological features in Uganda, though not included in this study, include:

- Cataclasites: Associated with the Aswa shear zone, extending over 300 km within Precambrian rocks.
- Metamorphic Rocks: Present extensively in the northern and central regions, including the Archaean Gneissic-Granulitic Complex, Watian, Aruan, and Mirian Groups.
- Meta-Igneous Rocks: Dominating western and south-central Uganda as part of the supracrustal Buganda-Toro System.

2.2.1. Sampling design

Sampling was conducted in February/March 2024, which are typically dry months (UNMA, 2023). A stratified random design was employed to capture a variety of community water sources used for domestic purposes across and specifically within five distinct hydrogeological settings in Uganda. The country was divided into strata based on hydrogeological units mapped by the British Geological Survey (BGS, 2019), with each stratum representing a unique hydrogeological setting. The study primarily focused on representative and contrasting units in eastern and parts of central Uganda (cf. Fig. 1b, c), in part due to logistical constraints. Within each hydrogeological stratum, water sources were randomly selected in areas targeted on the basis of: (i) ensuring spatially representative sampling within each domain (Richards et al., 2020); (ii) consideration of feasibility of total site/sample numbers within each domain; and (iii) consideration of accessibility, availability and prevalence of particular water source types within a given area. For instance, only springs were sampled in hilly volcanic areas, where they are the primary accessible water sources.

The campaign included 74 community water sources from boreholes (BH; $n = 51$), protected springs (PS; $n = 20$), and piped groundwater systems (PH; $n = 3$). These sources covered the following hydrogeological settings: Precambrian metasedimentary (MS; $n = 30$), granulitic gneissic complex (GG; $n = 21$), unconsolidated sedimentary (SDM; $n = 10$), volcanics (VO; $n = 7$), and metavolcanics (MV; $n = 6$). This manuscript expands upon a preliminary subset of data recently presented (Muloogi et al., 2025).

2.2.2. Water sample collection and in-situ measurements

All sampling bottles (glass) used were cleaned prior to use by acid-washing with 10% HNO_3 for about 24 h, thoroughly rinsed with ultrapure deionised water (MilliQ grade), and baked at 450 °C. Groundwater sampling followed standard procedures described elsewhere by the co-authors (Polya et al., 2017; Polya and Watts, 2017; Richards et al., 2017, 2020). All boreholes and pumps, which were in regular use, were purged for approximately 2 min to obtain representative aquifer samples. In the field, samples were filtered using a Minisart cellulose membrane (0.45 μm pore size) into 60 mL bottles, then sealed with Parafilm (Richards et al., 2020). Sampling repeats ($n = 4$) were included to evaluate sampling consistency. Samples were stored at ~4 °C except during unavoidable situations such as during transit or power outages. Subsamples for cationic analyses were acidified with 2 % trace analysis-grade nitric acid upon arrival at the Manchester Analytical Geochemistry Unit (MAGU), The University of Manchester, due to transport restrictions on nitric acid.

Measurements of pH, electrical conductivity (EC), total dissolved solids (TDS), temperature, and oxidation-reduction potential (ORP, Ag/AgCl reference electrode) were made *in-situ* using a Myron L Ultrameter II™ 6PFC. Regular three-point calibrations were made at pH 4, 7, and 10 (NIST traceable standards), as well as with HI 7021 ORP solution. The standard redox potential (*Eh* with respect to Standard Hydrogen Electrode) was obtained by correcting the ORP value with the offset for the standard half-cell potential of the Ag/AgCl reference electrode at 25 °C.

2.2.3. Quantification of trace and major elements/ions

The concentrations of major and trace elements were determined at MAGU laboratories using inductively coupled plasma optical emission spectrometer (ICP-OES; Agilent 5800) and inductively coupled mass spectrometer (ICP-MS, single quad; Agilent 7700). Due to different optimal concentration ranges for analysis, the ICP-OES results were preferred for Na, K, Mg, Ca, Si, while ICP-MS results were used for Fe, Mn, As, Pb, Cd, Cr, and U.

Anions (SO_4^{2-}, NO_3^-, PO_4, NO_2^-, Cl^-, Br^-) were quantified by ion chromatography (IC; Dionex ICS5000 Ion Chromatograph with Dionex IonPac AS18 columns) at MAGU. HCO_3^- was estimated based on electroneutrality (i.e., charge balance assumed to be 0 to estimate inferred HCO_3^-). Inferred HCO_3^- concentrations were compared to laboratory-based Gran titration on 25 % of samples, selected to represent a range of HCO_3^- values, following protocols described elsewhere (Barringer and Johnsson, 1996; Rounds, 2012, Fig. 2S).

2.3. Data quality assurance and quality control

Quality assurance and quality control (QA/QC) procedures broadly followed the recommendations by Polya et al. (2017), and as described elsewhere (Pincetti-Zúniga et al., 2020; Polya et al., 2017; Richards et al., 2017, 2020). Inverse variance-weighted first-order linear models were applied to ICP-OES and ICP-MS calibration data (Miller and Miller, 2018). Certified reference materials (CRMs; hard and soft drinking water standards: LGC 6026 and LGC 6027 respectively) were included in each

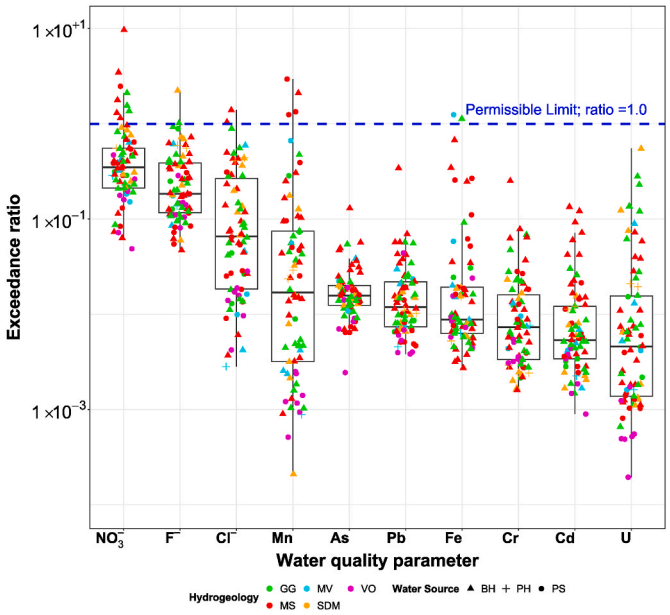

Fig. 2. Exceedance and box plots of selected parameters based on WHO (2017) drinking water guidelines. Y-axis is plotted on a log scale. The blue dashed line indicates concentrations equal to the guideline value (exceedance ratio = 1). Samples with concentrations above the guideline value are plotted above this line. Parameters are ordered by their median values, which are represented by horizontal lines within the boxes. The whiskers of the boxes represent 1.5 times the interquartile range (IQR). Colours represent hydrogeological units (GG – Granulitic Gneissic complex, MV – Metavolcanics, SDM – Unconsolidated sedimentary, VO – Volcanics, MS – Precambrian Metasedimentary), and shapes indicate different water sources (BH – Borehole, PH – Piped groundwater supply pumps, PS – Protected Spring). (For interpretation of the references to colour in this figure legend, the reader is referred to the Web version of this article.)

ICP-OES and ICP-MS analytical run, while QC1364, LGC 6020, and VHG-ICM1 500 (UK) were incorporated into IC analytical runs to assess potential biases. Duplicate analysis was performed on ~10 % of the samples ($n = 9$).

Concentrations of select analytes (SO_4^{2-}, F^-, PO_4, Na, K) that showed analytical biases greater than ± 10 % were corrected basing on a bias of a CRM selected to be in a similar concentration range of the target analyte. Specifically, LGC 6020 was used for SO_4^{2-} and F^-, VHG-ICM1 500 for PO_4, and LGC 6026, for Na and K.

General consistency was observed between alkalinity inferred by electroneutrality and via Gran titration, although two samples had negative inferred HCO_3^- values from electroneutrality calculations, which may be due to underestimation of positive ions or contributions from unmeasured minor negative ions. In these limited cases, the inferred values were replaced with Gran titration values for all the subsequent analyses.

2.4. Data processing and statistical tests

Data processing, statistical analyses, and graphics were performed using R (4.4.0) in R Studio (2024.04.0 + 735). Values below the detection limit (BDL) were imputed as half the lowest detected value for the respective parameter to allow inclusion in statistical analyses. The Shapiro-Wilk test (Shapiro and Wilk, 1965) was used to test if data was normally distributed. Correlation of selected variables was assessed using a Spearman rank-correlation test, which is appropriate for non-normal data distributions. A non-parametric Kruskal-Wallis test (Kruskal and Wallis, 1952) was used to compare mean concentrations across hydrogeological settings. A post-hoc Dunn's test was used for pairwise statistical comparison of concentrations across hydrogeological settings using a Bonferroni correction factor ($\frac{\alpha}{n}$), where n = the number of hypotheses tested (Dunn, 1964). All statistical tests were conducted at a 95 % confidence level ($\alpha = 0.05$).

Multivariate statistical analyses, in form of principal components analysis (PCA) and hierarchical cluster analysis (HCA), were performed in R using prcomp and hclust functions respectively, and visualised using the factoextra package (Kassambara, 2016) to identify relationships between water quality and potential explanatory variables (*e.g.* hydrogeological settings and water sources). PCA and HCA were performed on standardised/scaled water quality parameters across the overall dataset (mean = 0, variance = 1) to ensure equal contribution from all variables. In HCA, the distance matrix was computed using the Euclidean distance metric, and hierarchical clustering was performed using the Ward method (Ward Jr, 1963). The results were visualised as a dendrogram, with four clusters as optimal, as determined by both the Elbow and Silhouette methods.

2.5. Drinking and irrigation water quality assessment

A drinking-water quality assessment was conducted on all samples based on selected key water parameters outlined in the World Health Organization (WHO) provisional guideline values for drinking-water quality (WHO, 2017). All sampled sites were active community drinking-water sources, although are also used for other domestic purposes like washing and cooking. In all cases, the water is directly piped to users without prior treatment. Irrigation water quality was assessed using the U.S. Salinity Laboratory classification system (USSL, 1954).

2.6. Geochemical modelling

The Geochemist's Workbench® (GWB) 2023 Community Edition and PHREEQC interactive software (version 3.7.3) were used for geochemical modelling (Bethke, 2022; Parkhurst and Appelo, 1999). GWB was utilised to characterise water by means of Piper and Durov diagrams, calculated saturation indices and stability diagrams (with the *thermo.tdat* database). PHREEQC, using the *Phreeqc.dat* database, calculated ion activities across all samples using selected input parameters such as Ca, K, Si, Na, pH, and temperature. Ion concentrations were provided in mmol/kgw, temperature in °C, while pH were entered as unitless values.

3. Results and discussion

3.1. QA/QC results

Analytical biases indicated by analysis of CRMs (Table 1S) were within ±10 % for most analytes (Ca, Mg, Si, Mn, Fe, Mn, U, Pb, As, Cr, Cd, Cl^-, NO_3^-); for K, Na, SO_4^{2-}, F^-, PO_4, biases exceeded ± 10 % and corrections were applied accordingly (cf., Section 2.4). Analytical repeats for most analytes (Cl^-, Na, Mg, Ca, K; Table 2S), showed low coefficients of variation (CVs, 1 – 2 %). High CVs were observed for Fe (27 ± 16 %), and PO_4 (19 ± 16 %). Similarly, for the sampling repeats (Table 2S), the CVs were typically low (1 – 7 %) for most of the major ions, but higher for NO_2^- (54 ± 44 %), SO_4^{2-} (28 ± 56 %), and NO_3^- (18 ± 34 %). The observed variability, particularly for Fe, As, Cd, Pb, U, PO_4, NO_2^-, SO_4^{2-}, and NO_3^-, reflect measured concentrations near detection limits where errors are higher (Ellison et al., 2017; Ramsey, 1998).

A Wilcoxon test showed no significant overall difference between inferred and Gran titration HCO_3^- values ($p = 0.949$; $W = 129$; Fig. 2S), indicating general consistency across most samples. However, some deviations in limited individual samples may be impacted by degassing during storage, reduced accuracy of Gran titration at high alkalinity (Rounds and Wilde, 2012) and/or cumulative analytical uncertainties.

3.2. Hydrochemistry of water samples

3.2.1. In-situ physicochemical parameters

The samples showed variability in *in-situ* physicochemical parameters across different hydrogeological settings (Table 3S). Measured pH ranged from 5.8 to 8.4 (median 7.1), with highest values in VO, and the lowest in MS and GG. Electrical conductivity (EC: 49 – 1580 µS/cm; median 350 µS/cm) and TDS (34 – 1110 mg/L; median 230 mg/L) were highest in SDM and lowest in VO. All waters were oxidising, with *Eh* values (with respect to Standard Hydrogen Electrode) ranging from 237 to 497 mV (median 327 mV). Across hydrogeologies, VO samples had the highest *Eh* while SDM samples had the lowest.

3.2.2. Major and trace elements

The major cationic analytes and Si, had the following overall pattern of decreasing median concentrations: Si (1 – 72 mg/L; median 35 mg/L) > Ca (3 – 254 mg/L; median 25 mg/L) > Na (4 – 211 mg/L; median 20 mg/L) > Mg (1 – 119 mg/L; median 9 mg/L) > K (1 – 56 mg/L; median 4 mg/L), with noticeable variations across hydrogeological settings (Table 3S; Section 3.4). Anionic analytes exhibited the general pattern: HCO_3^- (13 – 560 mg/L; median 91 mg/L) > SO_4^{2-} (0.3 – 330 mg/L; median 26 mg/L) > NO_3^- (<0.02 – 480 mg/L; median 16 mg/L) > Cl^- (0.7 – 350 mg/L; median 15 mg/L) > F^- (0.1 – 3.4 mg/L; median 0.3 mg/L) > PO_4 (<DL – 4.8; median 0.2 mg/L) > Br^- (<DL – 1.1 mg/L; median 0.1 mg/L) > NO_2^- (<DL – 0.7 mg/L; median 0.02 mg/L), where DL is the detection limit.

Other selected elements, including some of particular health relevance (*e.g.* As, Cr, U, Pb, Cd), had generally low concentrations, following the overall pattern in order of decreasing median concentration: Mn (0.1–1180 µg/L; median 6 µg/L) > Fe (0.8 – 370 µg/L; median 3 µg/L) > Cr (0.1 – 13 µg/L; median 0.3 µg/L) > As (0.02 – 1.3 µg/L; median 0.2 µg/L) > U (0.01 – 17 µg/L; median 0.1 µg/L) > Pb (0.04 – 3 µg/L; median 0.1 µg/L) > Cd (0.0 – 0.4 µg/L; median 0.02 µg/L). Concentrations of likely geogenic Mn and Fe are broadly consistent with the pattern expected in moderately oxidising, circum-neutral waters (Xu and Li, 2024; Zhai et al., 2021), where Mn is more soluble than Fe due to its higher oxidation threshold, while Fe precipitates as insoluble oxides/hydroxides (Hem, 1972).

3.3. Drinking and irrigation water quality

3.3.1. Drinking water quality

Generally, low proportion of samples exceeded WHO drinking water (provisional) guidelines for selected health-based and/or operational targets (F^-, NO_3^-, Cl^-, Mn, Fe, Pb, Cr, Cd, As, and U) (Fig. 2). Overall, 3 % of samples exceeded Fe, F^-, and Cl^- limits, 5 % for Mn, while 14 % exceeded the NO_3^- limit. Exceedances varied by hydrogeological setting, with 20 % of samples in MS exceeding NO_3^-, 13 % exceeding Mn, and 7 % exceeding Cl^-. In GG, 14 % exceeded NO_3^-, and 5 % exceeded Fe. In MV, 17 % exceeded Fe, while in SDM, 10 % exceeded F^-, with no other exceedances. Across all settings, all samples were within (provisional) guideline values for As, Pb, Cr, Cd, and U. No exceedances were observed in VO setting.

The observed exceedances reflect a combination of anthropogenic and geogenic influences. Elevated NO_3^-, particularly in the MS and GG settings, likely results from human activities such as agricultural runoff, urban-derived inputs, and poor sanitation, which predominantly affect the country's shallow groundwater (Lapworth et al., 2017; Nyenje et al., 2014; Wilson et al., 2024a, 2024b). In contrast, elevated Mn and Fe concentrations are primarily geogenic, arising from the natural weathering of the host rocks in these settings, with local redox conditions and aquifer mineralogy potentially controlling their mobilisation (Bakyayita et al., 2019; Lapworth et al., 2020).

3.3.2. Irrigation water suitability

Most water samples fall within the C1–S1 to C3–S1 categories (Fig. 3S a), indicating low to moderate salinity and acceptable sodium levels for irrigation. C1–S1 (low salinity, low sodium) is suitable for all crops, while C2–S1 (medium salinity, low sodium) is suitable for most crops. C3–S1 (higher salinity) is suitable for salt-tolerant crops such as sorghum, cassava, and sugarcane (Adhikari et al., 2015; Leliveld et al., 2013), but high salinity can harm less salt-tolerant crops, like NERICA upland rice varieties grown in this region (MAAIF, 2009; Zaidi et al., 2015).

Some borehole samples in SDM (20 %), MS (10 %), and GG (10 %) regions exceeded a magnesium hazard ratio of 1 (Fig. 3S b), indicating elevated magnesium levels that could affect soil structure, reducing its permeability (Oster et al., 2016). Most samples had acceptable Soluble Sodium Percent (SSP), except for two spring and borehole sources, suggesting minimal sodicity impacts on soil.

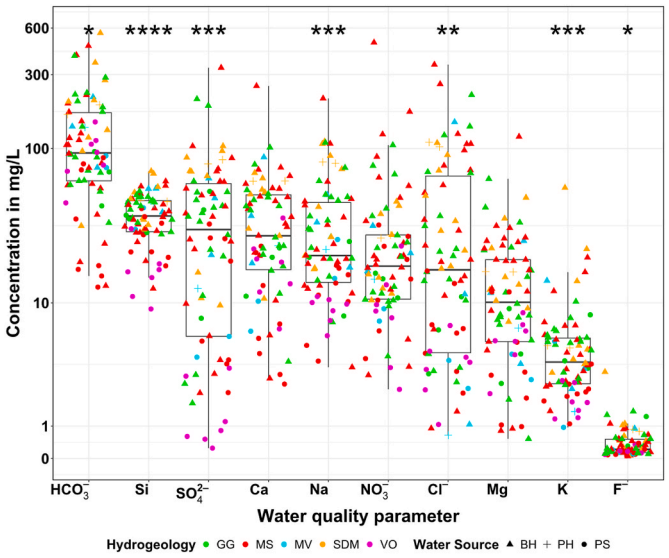

Fig. 3. Distribution of key water quality parameters (in mg/L) across different hydrogeological settings. Colours represent hydrogeological units (GG – Granulitic Gneissic complex, MV – Metavolcanics, SDM – Unconsolidated sedimentary, VO – Volcanics, MS – Precambrian Metasedimentary), and shapes indicate different water sources (BH – Borehole, PH – Piped groundwater supply/Pumps, PS – Protected Spring). Statistical significance (Kruskal-Walli's test) is shown for each parameter, if at least one hydrogeological setting is significantly different (**** for $p < 0.0001$; *** for $p < 0.001$; ** for $p < 0.01$; * for $p < 0.05$; left blank for no significant difference without Bonferroni correction). The box and whisker plots are arranged in order of decreasing median concentration for the analytes. (For interpretation of the references to colour in this figure legend, the reader is referred to the Web version of this article.)

3.4. Hydrogeochemical patterns across hydrogeological settings

The major ionic analytes, as well as Si, varied across hydrogeological settings (Table 3S; Fig. 3). Generally, the SDM exhibits the highest concentrations of Ca, K, Mg, Na, Cl^-, SO_4^{2-}, F^-, and HCO_3^-, suggesting active mineral dissolution. This is likely driven by the high porosity and permeability, typical of the country's unconsolidated sediments (Owor et al., 2018), facilitating rapid water flow. Although fast-moving water would generally reduce water-rock interactions, it continuously introduces fresh, undersaturated water to mineral surfaces, maintaining a chemical gradient that sustains more dissolution (Guo et al., 2023). Additional processes such as ion exchange and evaporation may further contribute. Conversely, MS shows the greatest variability in Ca, Mg, and Na, pointing to diverse geochemical influences from the heterogeneous mineralogy and structural complexity of metamorphic-sedimentary rocks (Nyakairu et al., 2002; Schlüter, 2008), leading to differential weathering and ion release.

Fluoride levels are most variable in SDM and least in VO. High

fluoride in some SDM sites likely reflects the occurrence of fluorite and other fluoride-bearing accessory minerals such as apatite, micas like biotite and muscovite within the local granitic or felsic sediments (Edmunds and Smedley, 2013).

The VO setting consistently shows lower concentrations of K, Cl^-, SO_4^{2-}, and HCO_3^-, likely due to the dominance of Neogene volcanic rocks with limited weathering potential, underlain by a resistant granite-gneiss basement (Westerhof et al., 2014). In addition, all samples from volcanic areas were collected from springs, which are associated with rapid flow rates, and shorter residence times, resulting in limited rock-water interactions.

Si levels, following the trend SDM > MV > GG > MS > VO, reflect variations in silicate weathering rates or the distribution and extent of felsic rocks across the different hydrogeological settings. Meanwhile, the low mean TDS values (<500 mg/L) across settings, are indicative of fresh groundwater and potential silicate weathering influences (Hounslow, 1995; Tay, 2012).

NO_3^- levels were highest in MS, suggesting anthropogenic contamination, as the sampled sites in this setting were predominantly within and around Jinja City. Given the nature of land use in the area, urban-derived inputs, faecal output from pit-latrines, and nutrient leaching from synthetic fertilisers used in the nearby intensive sugarcane agriculture are the most plausible contributors (Arwenyo et al., 2017; IFDC and AFAP, 2018; Wilson et al., 2024b).

For the trace elements, Mn concentrations were generally higher than Fe in GG, MS and SDM, whereas the converse was observed in VO and MV. This pattern reflects differences in aquifer lithological composition and localised redox conditions that influence their relative abundance in solution (Brown et al., 2003; Hamer et al., 2020). Mn is commonly mobilised in groundwater through reductive dissolution of Manganese (hydr)oxides, a process that can occur even under (sub) oxic conditions, releasing Mn^{2+} into solution (Jun and Martin, 2003). In contrast, Fe^{3+} reduction typically requires more strongly reducing conditions. Speciation modelling (Fig. 4S) indicates that Mn^{2+} is the dominant thermodynamically stable Mn species, whereas Fe is predominantly stable as hematite. This suggests that groundwater conditions generally favour Fe oxide stability, limiting dissolved Fe, but do not favour Mn oxide stability, allowing Mn^{2+} to persist in solution. Samples with elevated Fe likely reflect a combination of localised reductive dissolution of Fe(III) oxides, mobilisation of colloidal and organically complexed Fe within the saprolite and lateritic horizons (Brown et al., 2003), and contributions from corroded galvanised iron components in pipes (Casey et al., 2016).

Pairwise comparisons (Table 4S) show statistically significant differences for several parameters across different settings: K (SDM > VO, GG > VO), Si (multiple comparisons), Cl^- (SDM > VO), and SO_4^{2-} (multiple comparisons). Mn differs between MS > VO. F^- concentrations significantly vary (Fig. 3; Kruskal-Wallis, $p < 0.05$), but Bonferroni-corrected statistical tests reveal no significant differences ($p = 0.05$), except between SDM > VO ($p = 0.03$), indicating a relatively uniform distribution overall.

3.5. *Dominant geochemical conditions and geochemical evolution across contrasting hydrogeologies*

A Piper plot (Fig. 4a) was used to highlight dominant hydrochemical facies across hydrogeologies, while a Durov plot (Fig. 4b) informed understanding of geochemical evolution. Consistent with regional studies in Uganda (Guma et al., 2021; Owor et al., 2021; Taylor and Howard, 1995), HCO_3^- is the dominant anion, indicating limited geochemical evolution typical of shallow, discontinuous aquifers in crystalline rock environments (Chebotarev, 1955; Owor et al., 2021). Groundwater in this study is predominantly of the Ca–HCO_3 type, suggesting a stable signature characteristic of shallow, fresh groundwaters in equilibrium with local lithology. Owor et al. (2021) reported a dominance of Ca–Mg–HCO_3, a facies closely related to Ca–HCO_3 observed here, in comparable settings based on early drilling-stage samples. The slightly higher Mg content in their samples may reflect site-specific differences in rock-mineral sources, although the early drilling-stage samples can also be influenced by transient drilling-related effects or drilling fluid contamination (Richards et al., 2015). Notably, these water types exhibit spatial variability across hydrogeological settings.

Owor et al. (2021) reported Ca–Mg–HCO_3 dominance in meta-sediments (25 %), granites (28 %), and sediments (43 %), with volcanic settings (31 %) showing Mg–Ca–HCO_3. In contrast, current data shows that in the VO settings, Ca–HCO_3 (86 %) predominates, with the Durov plot trending towards $HCO_3^- + CO_3^{2-}$, suggesting mineral dissolution involving carbonates and plagioclase minerals such as anorthite.

In GG settings, Ca–HCO_3 facies dominate (38 %), although Na–HCO_3, Na–SO_4, and Mg–HCO_3 facies suggest cation exchange, potential contributions from evaporite-derived solutes, and mixing. The

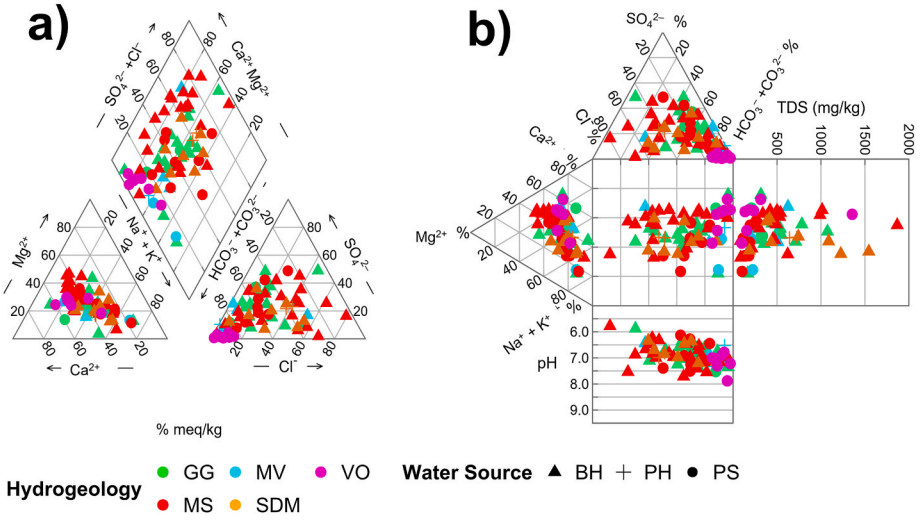

Fig. 4. a) - Piper diagram illustrating the hydrochemical facies and dominant water type on the samples; **b)** – Durov diagram illustrating the geochemical evolution of groundwater. Colours represent hydrogeological units (GG – Granulitic Gneissic complex, MV – Metavolcanics, SDM – Unconsolidated sedimentary, VO – Volcanics, MS – Precambrian Metasedimentary), and shapes indicate different water sources (BH – Borehole, PH – Piped groundwater supply pumps, PS – Protected Spring). (For interpretation of the references to colour in this figure legend, the reader is referred to the Web version of this article.)

Durov plot supports this, with some associated points trending toward $Na^+ + K^+$, indicating sodium enrichment.

In MS settings, Ca–HCO_3 (30 %) prevails, but Na–HCO_3 and Na–SO_4 facies suggest ongoing ion exchange, potential contributions from evaporite-derived solutes, and advanced geochemical evolution. The Durov plot trends toward Cl^- and SO_4^{2-}, consistent with mixing with sulphate-rich waters, likely reflecting minor contributions from residual evaporitic minerals or anthropogenic inputs. However, given the metamorphic nature of these units, any evaporitic influence is likely indirect and localised, with minimal input from bedded evaporites within the rocks.

In SDM settings, Na–Cl (40 %) predominates, alongside Na–SO_4, Ca–Cl, and other facies, potentially driven by a combination of evaporative concentration, cation exchange within clay-rich sediments, anthropogenic inputs supplying both Na^+ and Cl^-, and localised residual salinity in fine-grained lacustrine deposits; dissolution of bedded evaporites is very unlikely given the documented sedimentary stratigraphy (Westerhof et al., 2014). Although (semi)confined sedimentary aquifers, typical of those in Uganda (Owor et al., 2021) may, in principle, contain isolated saline connate waters (Langmuir, 1997), the predominantly shallow and hydraulically active nature of these aquifers suggests that near-surface concentration processes may exert a stronger control on groundwater salinity than long-term isolation from recharge.

In the MV settings, Na–HCO_3 (50 %) dominates, with some of the associated Durov points near $Na^+ + K^+$, reflecting the influence of cation exchange processes during aquifer freshening, whereby Ca^{2+} and Mg^{2+} are preferentially exchanged for Na^+ on mineral surfaces.

The observed spatial shifts in groundwater facies, and differences from earlier report by Owor et al. (2021), are attributed to site-specific factors *e.g.,* variations in well locations, and depths. However, it is also plausible that these shifts may reflect temporal changes in groundwater chemistry (due to mineral dissolution, cation exchange, water mixing; Dhar et al., 2008; Rajesh et al., 2012), and anthropogenic influences (*e.g.,* land use changes, groundwater extraction; Broers and van der Grift (2004)). Whilst this study does not quantify the effects of sustained abstraction or long-term chemical evolution, these remain plausible contributing mechanisms, particularly in impacted areas amidst the increasing demand. Active pumping or sustained extraction over a long period of time can create zones of active circulation, particularly in the unconfined or semi-confined aquifers, potentially driving the upward flow of older waters (Shand et al., 2007).

4. Delineating ionic sources and geochemical processes

4.1. Correlations of water quality parameters and implications

Correlations between selected water quality parameters (Fig. 5), were evaluated to investigate potential dominant geochemical processes and ionic sources influencing the groundwater chemistry. Strongest correlation was observed between Ca and Mg ($r = 0.93$), suggesting mineral dissolution, likely from carbonate sources such as limestone or from mafic and ultramafic rocks. This is supported by strong correlations between calcium, magnesium, and bicarbonate ($r = 0.75$ and 0.71, respectively).

Ca, Mg, Na, and K also showed strong correlations with Cl^-: Ca ($r = 0.78$), Mg ($r = 0.79$), Na ($r = 0.78$), and K ($r = 0.67$), consistent with co-mobilisation during water – rock interactions and/or anthropogenic inputs such as sewage in some settings. Further, significant correlations with SO_4^{2-}: Ca ($r = 0.77$), Na ($r = 0.78$), Mg ($r = 0.77$), and K ($r = 0.59$), point to shared geochemical processes, such as dissolution of sulphidic-minerals or anthropogenic inputs, introducing SO_4^{2-} alongside the cations.

The correlation of K with Na (r = 0.73) reflects their similar behaviour in response to environmental factors, allowing co-transport in groundwater systems (Redwan and Abdel Moneim, 2016). Ion exchange processes, where sodium or potassium replaces calcium and magnesium

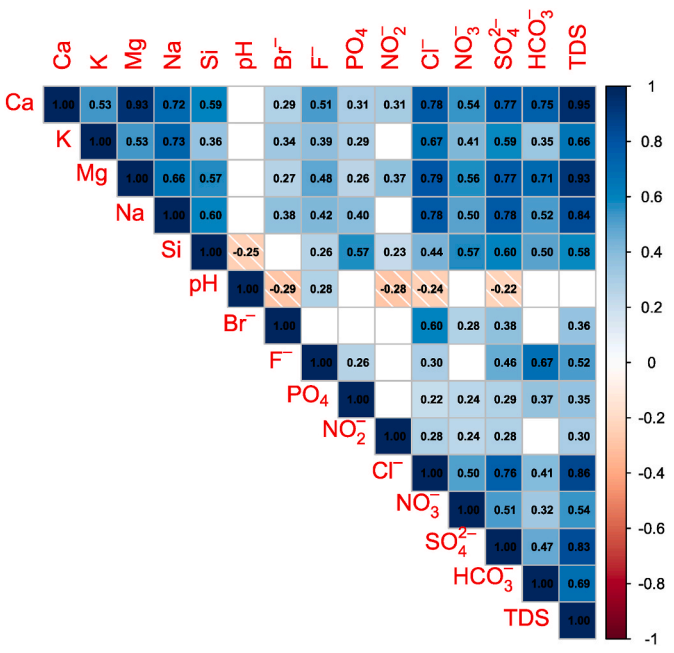

Fig. 5. A Spearman's rank correlation matrix of key water quality parameters computed using data from all hydrogeological settings. Each cell in the matrix shows a correlation coefficient, with only statistically significant correlations ($p < 0.05$) displayed, while insignificant correlations are left blank. Correlation strength is visually represented through shading (darker shading is a stronger correlation) and the *r* values within each cell.

in clays, may also contribute to their concentrations.

The strong correlations between Si and HCO_3^- (r = 0.5), Na (r = 0.6), and Ca (r = 0.59) suggest a likelihood of incongruent dissolution of feldspar minerals. Bromide and chloride (r = 0.73) are also strongly correlated, reflecting their conservative nature (Davis et al., 1998).

4.2. Multivariate analyses to decipher ionic sources and influences across hydrogeologies

Uganda's groundwater chemistry reflects geogenic processes and potential anthropogenic influences, as revealed by the PCA biplot and dendrogram (Fig. 6a, b). The first two principal components explain 62.3 % of the variance (cf. Fig. 5S), with major ions (HCO_3^-, SO_4^{2-}, Cl^-, Na, Ca, and Mg) strongly associated with the positive PC1 axis, along which borehole samples predominantly cluster. This association suggests a dominant control of water-rock interaction and mineral dissolution, with the positive co-variation of these ions, indicating shared geogenic sources. However, NO_3^- and SO_4^{2-}, despite aligning with the positive PC1 axis, may also reflect anthropogenic inputs, particularly in settings influenced by land use and sanitation (Wilson et al., 2024a).

Hierarchical clustering further distinguishes groups of geochemical indicators (HCO_3^-, SO_4^{2-}, Na, Cl^-, Ca, Mg, and TDS), representative of natural water-rock interactions, from contaminants (NO_3^-, NO_2^-, PO_4, and K), which are likely associated with agricultural fertilisers (*e.g.*, NPK; IFDC and AFAP, 2018; Luswata and Mbowa, 2015), and urban-derived pollution (Lapworth et al., 2017; Wilson et al., 2024a, 2024b).

Notably, fluoride showed positive associations with both HCO_3^- and Na, consistent with the increased solubility of fluorite in Na-rich waters through base exchange processes that reduce Ca^{2+} concentrations. This pattern aligns with global and regional observations that Na–HCO_3 water types can enhance fluoride release from fluorite and other fluorine-bearing accessory minerals (Edmunds and Smedley, 2013; Haji et al., 2018; Rusiniak et al., 2021). In addition, Na and SO_4^{2-} align together in C2, suggesting potential contributions from domestic

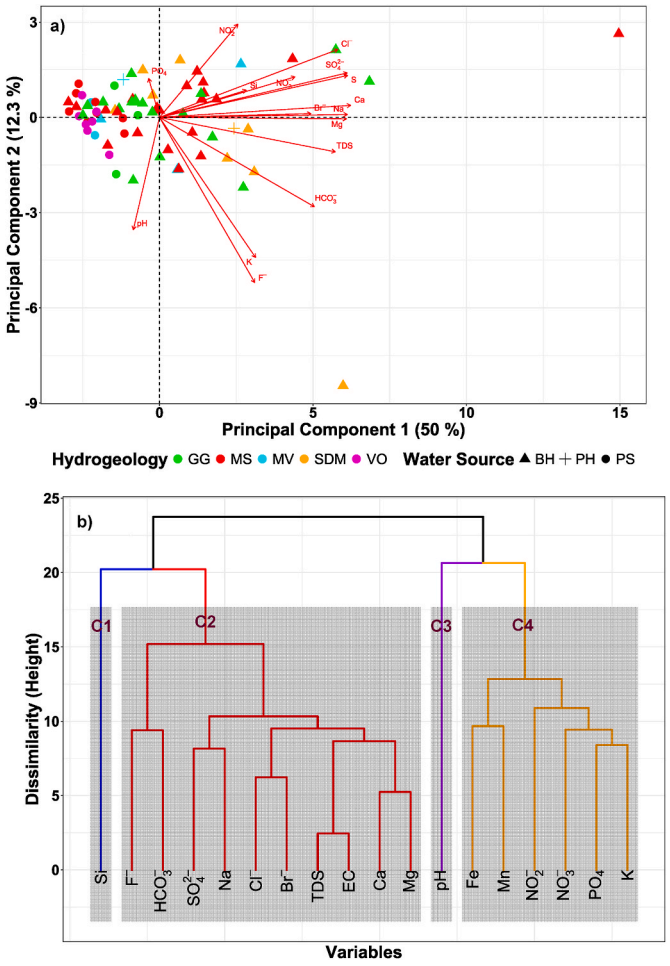

Fig. 6. a) Principal Component Analysis (PCA) biplot showing the relationships among various water quality parameters across different hydrogeologies and water sources. Colours represent hydrogeological units (GG – Granulitic Gneissic complex, MV – Metavolcanics, SDM – Unconsolidated sedimentary, VO – Volcanics, MS – Precambrian Metasedimentary), and shapes indicate different water sources (BH – Borehole, PH – Piped groundwater supply pumps, PS – Protected Spring). The axes represent the first two principal components, explaining 50 % and 12.3 % of the total variance, respectively, **b) -** Dendrogram illustrating the hierarchical clustering of Water Quality Parameters across the overall dataset based on scaled activity ratios. The plot shows four distinct clusters (C_1–C_4), determined by silhouette and elbow analyses, with branches coloured according to cluster membership. The dissimilarity in height indicates the degree of similarity between parameters. (For interpretation of the references to colour in this figure legend, the reader is referred to the Web version of this article.)

wastewater sources, including laundry detergents (Bajpai, 2007), especially in the urban or peri-urban settings. A detailed investigation of the impact of land use and anthropogenic influences on these ions is a topic of ongoing research by co-authors and extends beyond the scope of this manuscript.

4.3. Mechanisms and geochemical processes influencing groundwater chemistry

Most groundwater samples fall within the rock-weathering zone, indicating that rock–water interactions predominantly control groundwater chemistry (Fig. 7; Gibbs, 1970). This observation is consistent with the regional findings by Guma et al. (2021) and Owor et al. (2021), as well as Nyakairu et al. (2023) in the Kibiro springs.

Cation exchange and silicate hydrolysis generally outweigh halite dissolution as primary sources of Na, as most samples plot above or below the 1:1 line, with exceptions in MS and SDM (Fig. 8a). This interpretation is supported by mean $(Na^+ + K^+)/Cl^-$ ratios >1 across all hydrogeologies (Table 1), highest in MV and lowest in SDM, which is consistent with minimal evaporative concentration.

Carbonate dissolution is notable and may occur concurrently with silicate hydrolysis, for example Ca-rich plagioclase incongruent dissolution, as several samples plot close to the theoretical 1:2 line (Fig. 8b). Deviations from this trend, especially in GG and MS, suggest the influence of additional ion exchange processes.

Gypsum dissolution is minimal, with most samples above the 1:1 gypsum line except in GG and MS (Fig. 8c). $(Ca^{2+}+Mg^{2+})/SO_4^{2-}$ ratios (>1; Table 1), particularly in VO, are consistent with the observation by Westerhof et al. (2014), who noted that evaporites like gypsum are more common in semi-arid areas than in tropical, rainfall-fed regions like those sampled in this study. Thus, the calcium-sulphate correlation (Fig. 5) likely reflects the dissolution of other sulphate-bearing sources – potentially of anthropogenic origin – other than gypsum alone.

Cation exchange processes are indicated by inverse paired changes in alkali and alkaline earth cations (Fig. 8d). The dominance of Ca and Mg over Na and K, especially in MS and VO (Table 1; Fig. 6S), suggests a plausible contribution from reverse cation exchange in addition to other Ca and Mg sources. In contrast, the lower $(Ca^{2+} +Mg^{2+})/(Na^+ + K^+)$ ratios and Na-dominant facies in SDM and MV suggest a greater influence of cation exchange and progressive geochemical evolution, alongside other Na and K bearing sources such as silicates.

Silicate weathering relative to carbonate dissolution is further reflected in low-to-moderate HCO_3^-/Na^+ ratios (~1–4; Table 1), highest in VO and lowest in SDM. Notably, most samples are clustered at lower Ni/Cr ratios (Le Vaillant et al., 2016), even with increasing HCO_3^- levels (Fig. 7S a), suggesting that felsic rocks, rather than mafic or ultramafic sources, dominate incongruent dissolution. The Na-normalized plots (Fig. 8-e; Gaillardet et al., 1999) further support the predominance of silicate weathering with minimal evaporite dissolution. Deviations from end-member ratios indicate additional modifications, particularly by ion-exchange processes that alter the relative abundances of the major cations.

4.4. Geochemical behaviour and equilibrium states: saturation indices and stability of dominant mineral phases

The saturation indices (SI) for various mineral phases were examined to assess thermodynamic equilibrium conditions and to infer the potential for mineral dissolution or precipitation during geochemical interaction with aquifer host minerals (Fig. 9). Stability diagrams for feldspars, representing key silicates in the aquifer host rocks, were constructed to evaluate mineral stability and infer weathering trends across different hydrogeological settings (Fig. 10).

4.4.1. Saturation indices of the mineral species and implications

The saturation indices (SIs) for calcite and dolomite are mostly negative, indicating widespread thermodynamic undersaturation with respect to these minerals and potential dissolution in the aquifer matrix (**Eq. [1] and [2]**). However, calcite SIs exceed 0 in some samples from MS, SDM, and VO, suggesting localised supersaturation. Similarly, while dolomite is generally undersaturated, supersaturation occurs in samples from these settings and in GG. This occasional supersaturation likely reflects site-specific geochemical conditions, such as lower CO_2 partial pressures (Benavente et al., 2015; Drever, 1988; Fussmann et al., 2020).

In addition, supersaturation may be influenced by the common ion effect, particularly through Ca^{2+} enrichment from gypsum dissolution, other Ca-bearing minerals, or water mixing processes (Langmuir, 1997). Notably, the geochemical behaviour of dolomite and calcite appears similar, as indicated by a strong relationship between their SIs (Fig. 7S b). Dolomitization, however, is unlikely, as the Mg/Ca ratio remains low (<1) across all samples. Moreover, the consistently high Ca/Mg ratios

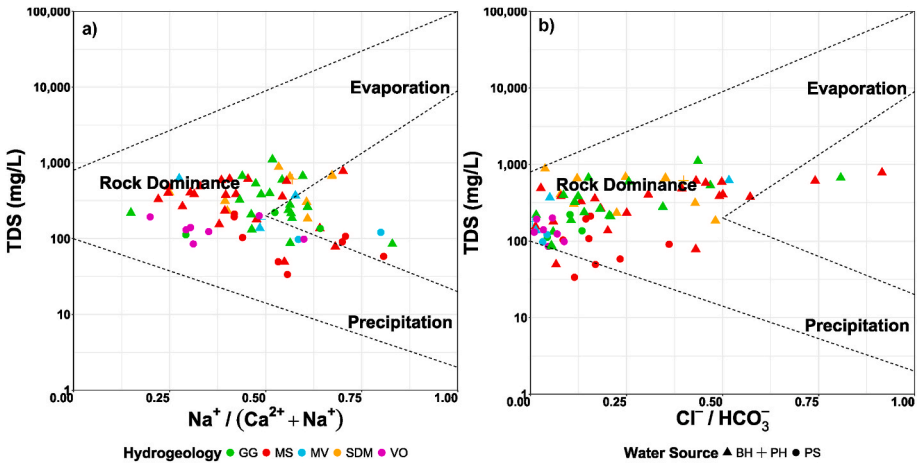

Fig. 7. Gibbs diagrams (Gibbs, 1970) showing the relationship between water chemistry and TDS across different water sources and hydrogeologies. **a**) -TDS Vs $Na^+/(Ca^{2+} + Na^+)$; **b**)- TDS Vs Cl^-/HCO_3-. All ionic concentrations are in mg/L. Dashed lines mark the key zones of precipitation, evaporation, and rock-weathering dominance. Water sources (BH – Borehole, PH – Piped groundwater supply pumps, PS – Protected Spring) are distinguished by shape, while hydrogeological settings (GG – Granulitic Gneissic complex, MV – Metavolcanics, SDM – Unconsolidated sedimentary, VO – Volcanics, MS – Precambrian Metasedimentary) are represented by different colours. (For interpretation of the references to colour in this figure legend, the reader is referred to the Web version of this article.)

(>1) suggest that calcium primarily comes from the dissolution of calcite and other Ca-rich minerals, such as anorthite, in the surrounding rock formations (Mayo and Loucks, 1995,Fig. 7S c).

4.4.1.1. *Calcite dissolution*

$$CaCO_3\ (s) + CO_2\ (g) + H_2O\ (l) \rightarrow Ca^{2+}\ (aq) + 2HCO_3^-\ (aq). \quad [1]$$

4.4.1.2. *Dolomite dissolution*

$$CaMg(CO_3)_2\ (s) + 2CO_2\ (g) + 2H_2O\ (l) \rightarrow Ca^{2+}\ (aq) + Mg^{2+}\ (aq) + 4HCO_3^-\ (aq). \quad [2]$$

Gypsum, anhydrite, and halides (*e.g.*, halite) consistently show negative SI values across all samples, indicating undersaturation. This is typical for non-saline, freshwater environments, where low levels of $SO_4^{2-}$and Cl^- are present due to the ongoing dissolution of these evaporites rather than their precipitation (Eid et al., 2024; Getenet et al., 2023). Despite their dissolution, gypsum and halides are not the primary ion sources in the sampled waters, with their contribution to overall ion concentrations being minimal (**cf.** Fig. 8a–c).

4.4.1.3. *Gypsum dissolution*

$$CaSO_4{\cdot}2H_2O\ (s) \rightarrow Ca^{2+}\ (aq) + SO_4^{2-}\ (aq) + 2H_2O\ (l). \quad [3]$$

Interestingly, despite the general dominance of Ca as a major cation across the settings (**cf.** section 3.2.2), most samples remain undersaturated with respect to fluorite (CaF_2). This undersaturation reflects the generally low fluoride concentrations across all settings, insufficient to reach CaF_2 equilibrium. A few samples, however, approach saturation. In such cases, competing carbonate mineral equilibria become important. Precipitation of dolomite and calcite can lower dissolved Ca^{2+}, which in turn can promote fluorite dissolution and lead to localised enrichment of fluoride in groundwater (Edmunds and Smedley, 2013).

4.4.2. *Stability of feldspars*

Unlike the carbonates and evaporate minerals, whose saturation indices can be directly interpreted (cf., section 4.4.1), the equilibrium of aluminium silicates requires careful consideration. As Appelo and Postma (2004) noted, dissolved Al concentrations in near-neutral pH groundwater are typically low and difficult to measure accurately. Additionally, Al-hydroxy complexes may persist in solution and not be fully removed by filtration, leading to uncertainties in speciation models.

To address these uncertainties, mineral relative stability diagrams are used as they assume that Al is conserved in the mineral phases. These diagrams reveal that silicate weathering, through ion release from feldspars (albite, K-feldspar, and anorthite), which are widespread in Uganda's granulites and sediments (Schneider et al., 2016; Westerhof et al., 2014), influences groundwater chemistry by forming stable secondary mineral phases (Fig. 10). The incongruent dissolution equations are as follows:

Albite dissolution

$$2NaAlSi_3O_8\ (s) + 2H_2CO_3 + 9H_2O \rightarrow Al_2Si_2O_5(OH)_4 + 2Na^+\ (aq) + 2HCO_3^-(aq) + 4H_4SiO_4(aq) \quad [4]$$

K-Feldspar dissolution

$$2KAlSi_3O_8\ (s) + 2H_2CO_3 + 9H_2O \rightarrow Al_2Si_2O_5(OH)_4 + 2K^+\ (aq) + 2HCO_3^-(aq) + 4H_4SiO_4(aq) \quad [5]$$

Anorthite dissolution

$$CaAl_2Si_2O_8\ (s) + 2CO_2 + 3H_2O \rightarrow Al_2Si_2O_5(OH)_4 + Ca^{2+}\ (aq) + 2HCO_3^-(aq) \quad [6]$$

Most samples across all feldspars fall within the clinoptilolite stability field (*e.g.*, clinoptil-Na for Albite, Fig. 10 A; clinoptil-K for K-feldspar, Fig. 10 B; clinoptil-Ca for Anorthite, Fig. 10 C). Around 35 % of all samples, including ~40 % of VO samples, lie within the pyrophyllite field for albite. Few MS samples for Anorthite and none for K-feldspar fall within pyrophyllite. Most VO samples for Albite and anorthite trend towards the kaolinite field. Most samples are on the right side of the quartz saturation line, indicating supersaturation with respect to quartz, consistent with its supersaturation (cf. Fig. 9). Conversely, most samples are on the left of amorphous silica solubility line, indicating undersaturation, except for a few borehole samples in SDM, MS and MV settings.

The dominance of samples plotting within the clinoptilolite stability field suggests conditions favourable for zeolite formation. Zeolite deposits have been reported in eastern Uganda (Wangi et al., 2023), although the actual clinoptilolite occurrence in these aquifers is uncertain and its presence is theoretically modelled based on equilibrium conditions. Even at low abundance, clinoptilolite can influence groundwater chemistry by facilitating active ion exchange (Rodríguez-Iznaga et al., 2022).

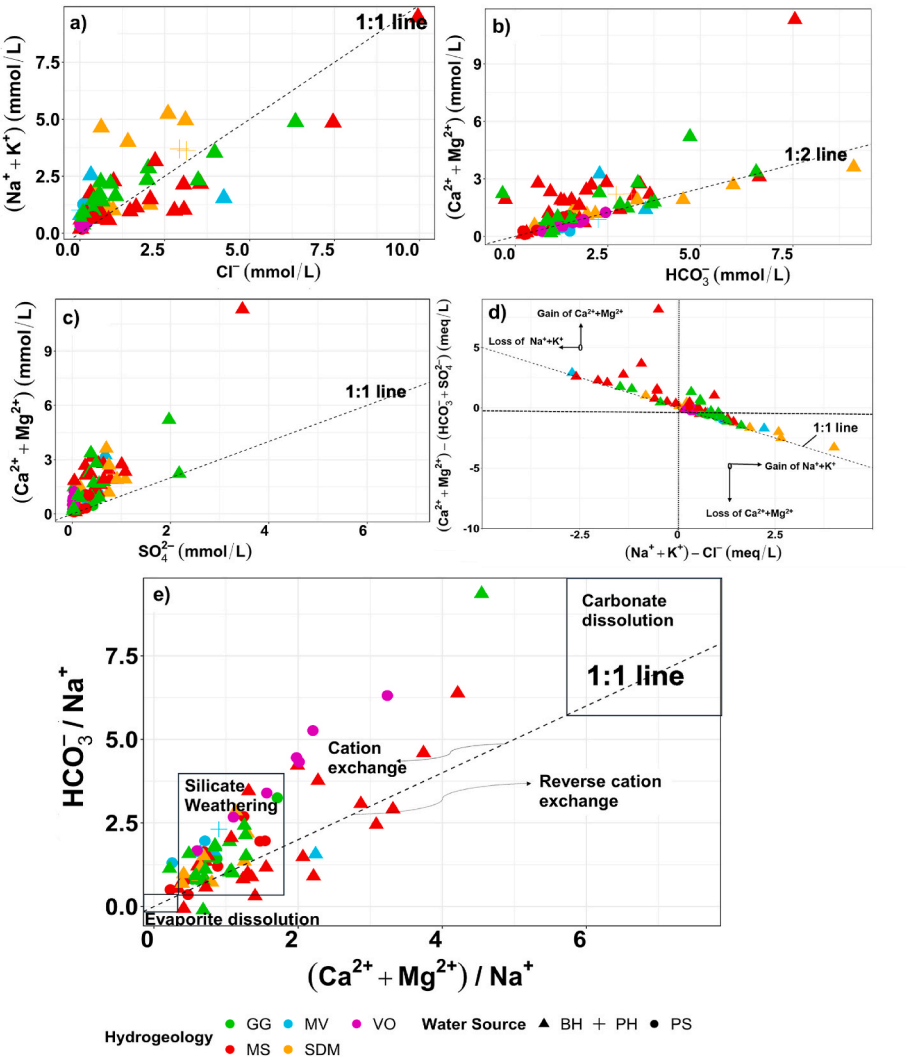

Fig. 8. Geochemical processes controlling groundwater chemistry across contrasting hydrogeological settings. Scatter plots show the relationships between key ion pairs for various processes: **(a)** - Evaporite Dissolution (($Na^+ + K^+$) vs Cl^-); **(b)** - Carbonate Weathering (($Ca^{2+} + Mg^{2+}$) vs HCO_3^-); **(c)** - Gypsum Dissolution (($Ca^{2+} + Mg^{2+}$) vs SO_4^{2-}); **(d)** - Cation Exchange (($Na^+ + K^+$) - Cl^-) vs ($Ca^{2+} + Mg^{2+}$) – ($HCO_3^- - SO_4^{2-}$)) (Blanchette et al., 2010; Fisher and Mullican, 1997); and **(e)**- representation of all geochemical processes (Molar $(HCO_3^-)/Na^+$) vs ($Ca^{2+} + Mg^{2+}$)/Na^+) (modified from Gaillardet et al., 1999). Dashed line is included to indicate an ideal stoichiometric relationship for dissolution processes. Different hydrogeologies are represented by distinct colours: GG – Granulitic Gneissic complex, MV – Metavolcanics, SDM – Unconsolidated sedimentary, VO – Volcanics, MS – Precambrian Metasedimentary. Water sources are indicated by different shapes: BH – Borehole, PH – Piped groundwater supply pump, PS – Protected Spring. (For interpretation of the references to colour in this figure legend, the reader is referred to the Web version of this article.)

Table 1
Mean major ionic ratios across contrasting hydrogeologies (HG) in Uganda. All ionic concentrations are in mmol/L.

HG	$(Na^+ + K^+)/Cl^-$	$(Ca^{2+} + Mg^{2+})/SO_4^{2-}$	$(Ca^{2+} + Mg^{2+})/HCO_3^-$	$(Ca^{2+} + Mg^{2+})/(Na^+ + K^+)$	HCO_3^-/Na^+
GG	3.4	6.4	0.3	1.0	1.8
MS	2.6	6.1	0.8	1.4	1.9
MV	17.5	5.3	0.6	0.9	1.7
SDM	2.3	4.4	0.7	0.7	1.3
VO	5.2	74.3	0.5	1.6	4.0

Samples plotting towards the pyrophyllite field reflect aquifers that have undergone substantial leaching, producing high dissolved silica relative to alkali and alkaline-earth cations. This chemical composition is consistent with long-term weathering of the low to medium-grade metamorphic basement of Uganda's older continental crust (Schlüter, 2008; Westerhof et al., 2014), where cations are preferentially leached while silica accumulates in solution, driving the system towards conditions that stabilise pyrophyllite. In contrast, VO samples occupying the kaolinite stability field, reflects monosiallitisation in well-drained environments (Gountié Dedzo et al., 2017; Langmuir, 1997; Tardy, 1971).

The limited gibbsite formation and observed monosiallitisation align with expected less aggressive post-Neogene weathering conditions (Modenesi-Gauttieri et al., 2011) characteristic of the prevalent Neogene rocks, particularly in the country's volcanic areas (Westerhof et al., 2014). In the VO setting, low dissolved silica levels reflect advanced silicate weathering of reactive volcanic rocks (Appelo and Postma, 2004), such as basalt and rhyolite in the Elgon volcanic region

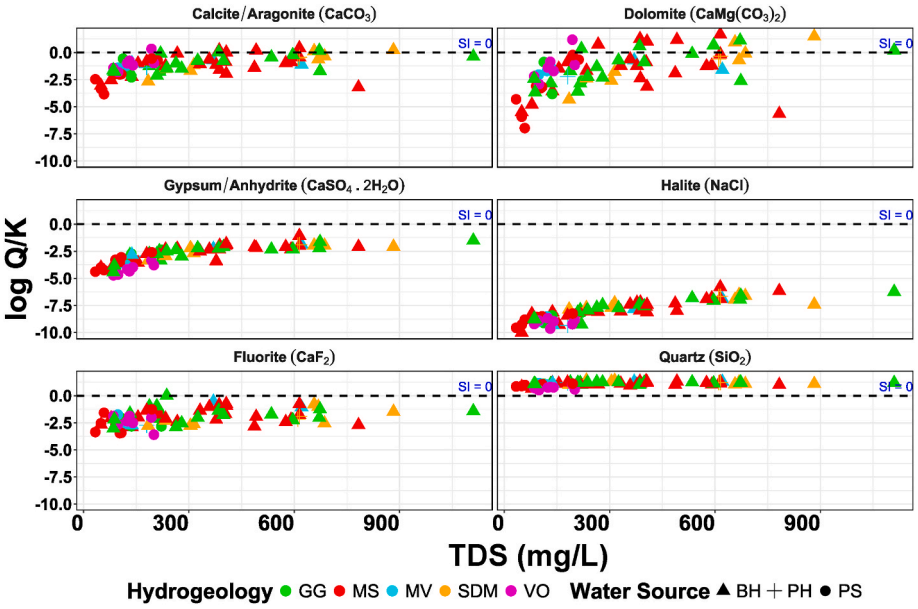

Fig. 9. Saturation indices (SI) of various minerals as a function of Total Dissolved Solids (TDS) across different water sources and hydrogeological settings. The minerals include carbonates (calcite, dolomite), gypsum (or anhydrites), halides (halite, fluorite), and quartz. Colours represent different hydrogeologies (GG – Granulitic Gneissic complex, MV – Metavolcanics, SDM – Unconsolidated sedimentary, VO – Volcanics, MS – Precambrian Metasedimentary) and shapes indicate water sources (BH – Borehole, PH – Piped groundwater supply pumps, PS – Protected Spring). The dashed horizontal line (SI = 0) indicates equilibrium between dissolution and precipitation for each mineral, where values above 0 signify supersaturation and values below 0 indicate undersaturation. (For interpretation of the references to colour in this figure legend, the reader is referred to the Web version of this article.)

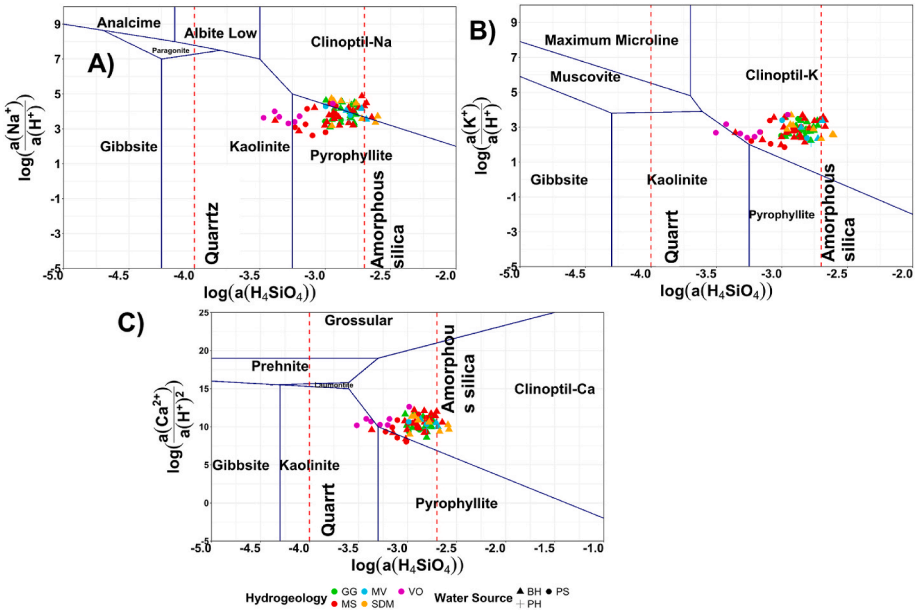

Fig. 10. Relative mineral stabilities plotted on (**A**) log (aNa^+/H^+); (**B**) log (aK^+/H^+); (**C**) ($aCa^{2+}/(H^+)^2$) vs log (a (H_4SiO_4) activity ratio diagrams. Points are shaped by water source (BH – Borehole, PH – Piped groundwater supply pumps, PS – Protected Spring) and coloured by hydrogeology (GG – Granulitic Gneissic complex, MV – Metavolcanics, SDM – Unconsolidated sedimentary, VO – Volcanics, MS – Precambrian Metasedimentary).

(Williams, 1969), with potential contributions from nepheline (Westerhof et al., 2014). The rapid flow within the sampled springs and corresponding lower silica accumulation favour kaolinite stabilisation, while other hydrogeologies likely experience less intense weathering, stabilising clinoptilolite and retaining higher dissolved silica.

5. Conclusion

Assessment of groundwater chemistry across Uganda's contrasting hydrogeological settings revealed distinct hydrogeochemical patterns. The SDM showed the highest major ion concentrations (Ca, Mg, Na, K Cl^-, F^-, SO_4^{2-}, and HCO_3^-), while VO exhibited the lowest, likely due to limited rock-water interactions and rapid flow rates. MS showed the greatest variability in Ca, Mg, and Na, consistent with heterogenous geochemical controls. Elevated NO_3^-, especially in MS groundwater, likely reflects anthropogenic contamination, noting detailed tracing of anthropogenic contributions is a topic of ongoing investigation.

Exceedances of (provisional) WHO guidelines values for selected

target analytes were relatively low; only 3 % of total samples surpassed limits for Fe, F^- and Cl^-, 5 % for Mn, while 14 % for NO_3^-. By hydrogeological settings, exceedances were: (i) MS – 20 % NO_3^-, 13 % Mn, and 7 % Cl^-; (ii) GG – 14 % NO_3^-, and 5 % Fe; (iii) MV –17 % Fe; and (iv) SDM – 10 % F^-.

Groundwater in Uganda is generally fresh and shallow, dominantly Ca–HCO_3 type, reflecting limited geochemical evolution typical of shallow, discontinuous aquifers. Exceptions occur in MV and SDM, where Na–HCO_3 and Na–Cl facies dominate respectively, consistent with cation exchange and advanced geochemical evolution. Despite the shallow nature of the groundwater, the weatherability of primary minerals strongly influences groundwater chemistry. Silicate (dominantly felsic) weathering, cation exchange, and carbonate dissolution contribute to baseline ion concentrations, while evaporative concentration and gypsum dissolution are minor across all settings. Most samples across all settings showed undersaturation for calcite, dolomite, gypsum, and halides, but supersaturation of quartz. Kaolinite is thermodynamically stable only in volcanics, where active monosiallitisation likely occurs, and the rapid water flow, well-drained conditions, and low silica content favour its stabilisation. In other settings, clinoptilolite is favoured, consistent with active cation exchange and early-to-intermediate stages of silicate weathering under higher dissolved silica conditions. These findings reveal diverse geochemical processes shaping Uganda's groundwater chemistry, emphasising the need for hydrogeologically-tailored groundwater monitoring and management.

CRediT authorship contribution statement

Derick Muloogi: Conceptualization, Data curation, Formal analysis, Investigation, Methodology, Visualization, Writing – original draft. **George J.L. Wilson:** Investigation, Methodology, Writing – review & editing. **Farah T. Ahmed:** Investigation, Writing – review & editing. **David A. Polya:** Conceptualization, Funding acquisition, Methodology, Supervision, Writing – review & editing. **Laura A. Richards:** Conceptualization, Funding acquisition, Investigation, Methodology, Project administration, Resources, Supervision, Writing – review & editing.

Declaration of competing interest

The authors declare that they have no known competing financial interests or personal relationships that could have appeared to influence the work reported in this paper.

Acknowledgements

We gratefully acknowledge support from The University of Manchester Dean's Doctoral Scholarship (to DM), a Dame Kathleen Ollerenshaw Fellowship (to LAR, including GW studentship), a UKRI Future Leaders Fellowship (MR/Y016327/1 to LAR et al.; www.aquaroad.org), and the Bangladesh Bangabandhu Science and Technology Fellowship Trust (FA studentship). We also thank the International Science Partnership Fund (ISPF) – England Project, awarded to LAR et al. via the University of Manchester (2023 – 2024), for supporting this project. Our appreciation goes to the Ministry of Water and Environment, Uganda – especially Caroline Wafula, Abudallah Matovu, and Alex Kyombo, the Jinja District Water Officer – for granting permissions to access community water points during our water sampling campaign. We also thank Yasin Koire for field support. Jonny Huck and Sam Shaw are thanked for discussions. Jordan Gaskell, Abby-Ragazzon Smith, and Rosie Byrne (all The University of Manchester) are acknowledged for their analytical support through MAGU. We thank the two anonymous reviewers for their constructive comments. The views expressed here do not necessarily represent those of the institutions, funders, or individuals whose support is acknowledged.

Appendix A. Supplementary data

Supplementary data to this article can be found online at https://doi.org/10.1016/j.apgeochem.2026.106738.

Data availability

Data supporting this study are provided in the manuscript and accompanying Supplementary Information.

References

Adhikari, U., Nejadhashemi, A.P., Woznicki, S.A., 2015. Climate change and eastern Africa: a review of impact on major crops. Food Energy Secur. 4, 110–132. https://doi.org/10.1002/fes3.61.

Agbasi, J.C., Abu, M., Pande, C.B., Uwajingba, H.C., Abba, S.I., Egbueri, J.C., 2025. Groundwater salinization in coastal regions and the control mechanisms: insights for sustainable groundwater development and management. In: Li, P., He, X., Wu, J., Elumalai, V. (Eds.), Sustainable Groundwater and Environment: Challenges and Solutions. Springer, Nature Switzerland, Cham, pp. 165–191. https://doi.org/10.1007/978-3-031-82194-3_8.

Appelo, C.A.J., Postma, D., 2004. Geochemistry, Groundwater and Pollution. CRC press. https://doi.org/10.1201/9781439833544.

Arwenyo, B., Wasswa, J., Nyeko, M., Kasozi, G., 2017. The impact of septic systems density and nearness to spring water points, on water quality. Afr. J. Environ. Sci. Technol. 11, 11–18.

Bajpai, D., 2007. Laundry detergents: an overview. J. Oleo Sci. 56, 327–340. https://doi.org/10.5650/jos.56.327.

Bakyayita, G.K., Norrström, A.C., Kulabako, R.N., 2019. Assessment of levels, speciation, and toxicity of trace metal contaminants in selected shallow groundwater sources, surface runoff, wastewater, and surface water from designated streams in Lake Victoria basin, Uganda. J. Environ. Public Health. https://doi.org/10.1155/2019/6734017, 2019.

Barringer, J.L., Johnsson, P.A., 1996. Theoretical Considerations and a Simple Method for Measuring Alkalinity and Acidity in low-pH Waters by Gran Titration (Water-Resources Investigations Report, vols. 89–4029.

Benavente, J., Vadillo, I., Liñán, C., Carrasco, F., Soler, A., 2015. A field analog of CO 2-closed conditions in a karstified carbonate aquifer (Nerja Cave experimental site, south Spain). Hydrogeol. Environ. Investig. Karst Syst. 533–542. https://doi.org/10.1007/978-3-642-17435-3_60.

Bethke, C.M., 2022. Geochemical and Biogeochemical Reaction Modeling. Cambridge university press.

BGS, G.Q., 2001. Br. Geol. Surv. Nottm. UK USA. Uganda, London. https://www2.bgs.ac.uk/groundwater/downloads/country_sheets/Uganda.

BGS, 2019. Africa Groundwater Atlas Country Hydrogeology Maps. British Geological Survey Open Report. https://www.bgs.ac.uk/geology-projects/africa-groundwater-atlas/.

Blanchette, D., Lefebvre, R., Nastev, M., Cloutier, V., 2010. Groundwater quality, geochemical processes and groundwater evolution in the Chateauguay River watershed, Quebec, Canada. Can. Water Resour. J. 35, 503–526. https://doi.org/10.4296/cwrj3504503.

Broers, H.P., van der Grift, B., 2004. Regional monitoring of temporal changes in groundwater quality. J. Hydrol. 296, 192–220. https://doi.org/10.1016/j.jhydrol.2004.03.022.

Brown, D.J., Helmke, P.A., Clayton, M.K., 2003. Robust geochemical indices for redox and weathering on a granitic laterite landscape in Central Uganda. Geochem. Cosmochim. Acta 67, 2711–2723. https://doi.org/10.1016/S0016-7037(03)00104-2.

Cahen, L., Snelling, N.J., Delhal, J., Vail, J.R., Bonhomme, M., Ledent, D., 1984. The Geochronology and Evolution of Africa. Lond. Oxf.

Casey, V., Brown, L., Carpenter, J.D., Nekesa, J., Etti, B., 2016. The role of handpump corrosion in the contamination and failure of rural water supplies. Waterlines 59–77. https://www.jstor.org/stable/26600753.

Chebotarev, I.I., 1955. Metamorphism of natural waters in the crust of weathering—1. Geochem. Cosmochim. Acta 8, 22–48. https://doi.org/10.1016/0016-7037(55)90015-6.

Davis, S.N., Whittemore, D.O., Fabryka-Martin, J., 1998. Uses of chloride/bromide ratios in studies of potable water. Groundwater 36, 338–350. https://doi.org/10.1111/j.1745-6584.1998.tb01099.x.

Dhar, R., Zheng, Y., Stute, M., Van Geen, A., Cheng, Z., Shanewaz, M., Shamsudduha, M., Hoque, M., Rahman, M., Ahmed, K., 2008. Temporal variability of groundwater chemistry in shallow and deep aquifers of Araihazar, Bangladesh. J. Contam. Hydrol. 99, 97–111. https://doi.org/10.1016/j.jconhyd.2008.03.007.

Drever, J., 1988. The Geochemistry of Natural Waters, vol. 437. Prentice hall, Englewood Cliffs.

Dunn, O.J., 1964. Multiple comparisons using rank sums. Technometrics 6, 241–252. https://doi.org/10.1080/00401706.1964.10490181.

Edmunds, W.M., Smedley, P.L., 2013. Fluoride in natural waters. In: Selinus, O. (Ed.), Essentials of Medical Geology, Revised Edition. Springer, Netherlands, Dordrecht, pp. 311–336. https://doi.org/10.1007/978-94-007-4375-5_13.

Egor, M., Birungi, G., 2020. Fluoride contamination and its optimum upper limit in groundwater from Sukulu Hills, Tororo district, Uganda. Sci. Afr. 7, e00241. https://doi.org/10.1016/j.sciaf.2019.e00241.
Eid, M.H., Eissa, M., Mohamed, E.A., Ramadan, H.S., Czuppon, G., Kovács, A., Szűcs, P., 2024. Application of stable isotopes, mixing models, and K-means cluster analysis to detect recharge and salinity origins in Siwa oasis, Egypt. Groundw. Sustain. Dev. 25, 101124. https://doi.org/10.1016/j.gsd.2024.101124.
Elango, L., Kannan, R., 2007. Rock–water interaction and its control on chemical composition of groundwater. Dev. Environ. Sci. 5, 229–243. https://doi.org/10.1016/S1474-8177(07)05011-5.
Ellison, S.L., Ramsey, M.H., Lawrance, P., Stuart, B., Minguez, J., Walker, M.J., 2017. Is measurement uncertainty from sampling related to analyte concentration? Anal. Methods 9, 5989–5996. https://doi.org/10.1039/C7AY00752C.
Fader, C.T., 2011. Retrofitting boreholes contaminated with iron in rural Uganda. https://doi.org/10.37099/mtu.dc.etds/516.
Fisher, R.S., Mullican, I., William, F., 1997. Hydrochemical evolution of sodium-sulfate and sodium-chloride groundwater beneath the Northern Chihuahuan desert, Trans-Pecos, Texas, USA. Hydrogeol. J. 5, 4–16. https://doi.org/10.1007/s100400050102.
Flynn, R., Taylor, R., Kulabako, R., Miret-Gaspa, M., 2012. Haematite in lateritic soils aids groundwater disinfection. Water. Air. Soil Pollut. 223, 2405–2416. https://doi.org/10.1007/s11270-011-1033-0.
Fussmann, D., von Hoyningen-Huene, A.J.E., Reimer, A., Schneider, D., Babková, H., Peticzka, R., Maier, A., Arp, G., Daniel, R., Meister, P., 2020. Authigenic formation of Ca–Mg carbonates in the shallow alkaline Lake Neusiedl, Austria. Biogeosciences 17, 2085–2106. https://doi.org/10.5194/bg-17-2085-2020.
Gaillardet, J., Dupré, B., Louvat, P., Allegre, C., 1999. Global silicate weathering and CO2 consumption rates deduced from the chemistry of large rivers. Chem. Geol. 159, 3–30. https://doi.org/10.1016/S0009-2541(99)00031-5.
Getenet, M., Otálora, F., Emmerling, F., Al-Sabbagh, D., García-Ruiz, J.M., 2023. Mineral precipitation and hydrochemical evolution through evaporitic processes in soda brines (East African Rift valley). Chem. Geol. 616, 121222. https://doi.org/10.1016/j.chemgeo.2022.121222.
Gibbs, R.J., 1970. Mechanisms controlling world water chemistry. Science 170, 1088–1090. https://doi.org/10.1126/science.170.3962.1088.
Gountié Dedzo, M., Tsozué, D., Ernestine Mimba, M., Teddy, F., Mofor Nembungwe, R., Linida, S., 2017. Importance of rocks and their weathering products on groundwater quality in Central-east Cameroon. Hydrology 4, 23. https://doi.org/10.3390/hydrology4020023.
Guma, B.E., Muwanga, A., Owor, M., 2021. Hydrogeochemical evolution and contamination of groundwater in the Albertine Graben, Uganda. Environ. Earth Sci. 80, 1–17.
Guo, H., Gao, Z., Xing, S., 2023. Water–rock interactions: mineral dissolution. Med. Geol. En Route One Health 111–127. https://doi.org/10.1007/s12665-021-09587-6.
Haji, M., Wang, D., Li, L., Qin, D., Guo, Y., 2018. Geochemical evolution of fluoride and implication for F− enrichment in groundwater: example from the bilate river basin of Southern main Ethiopian rift. Water 10. https://doi.org/10.3390/w10121799.
Hamer, K., Gudenschwager, I., Pichler, T., 2020. Manganese (Mn) concentrations and the Mn-Fe relationship in shallow groundwater: implications for groundwater monitoring. Soil Syst. 4, 49. https://doi.org/10.3390/soilsystems4030049.
Hem, J.D., 1972. Chemical factors that influence the availability of iron and manganese in aqueous systems. Geol. Soc. Am. Bull. 83, 443–450. https://doi.org/10.1130/0016-7606(1972)83[443:CFTITA]2.0.CO;2.
Hounslow, A., 1995. Water Quality Data: Analysis and Interpretation. CRC press. https://doi.org/10.1201/9780203734117.
Howard, G., Pedley, S., Barrett, M., Nalubega, M., Johal, K., 2003. Risk factors contributing to microbiological contamination of shallow groundwater in Kampala, Uganda. Water Res. 37, 3421–3429. https://doi.org/10.1016/S0043-1354(03)00235-5.
ICPAC, 2017. Africa administrative level. https://geoportal.icpac.net/catalogue/csw_to_extra_format.
IFDC, A.F.A.P., 2018. Assessment of fertilizer distribution systems and opportunities for developing fertilizer blends in Uganda. https://agra.org/wp-content/uploads/2020/08/Uganda-Report_Assessment-of-Fertilizer-Distribution-Systems-and-Opportunities-for-Developing-Fertilizer-Blends.
Jebreen, H., Banning, A., Wohnlich, S., Niedermayr, A., Ghanem, M., Wisotzky, F., 2018. The influence of karst aquifer mineralogy and geochemistry on groundwater characteristics: west bank, Palestine. Water 10, 1829. https://doi.org/10.3390/w10121829.
Jun, Y.-S., Martin, S.T., 2003. Microscopic observations of reductive manganite dissolution under oxic conditions. Environ. Sci. Technol. 37, 2363–2370. https://doi.org/10.1021/es026254x.
Kassambara, A., 2016. Factoextra: extract and visualize the results of multivariate data analyses. R Package Version 1. https://doi.org/10.32614/cran.package.factoextra.
Kisembe, J., Favre, A., Dosio, A., Lennard, C., Sabiiti, G., Nimusiima, A., 2019. Evaluation of rainfall simulations over Uganda in CORDEX regional climate models. Theor. Appl. Climatol. 137, 1117–1134. https://doi.org/10.1007/s00704-018-2643-x.
Kruskal, W.H., Wallis, W.A., 1952. Use of ranks in one-criterion variance analysis. J. Am. Stat. Assoc. 47, 583–621. https://doi.org/10.1080/01621459.1952.10483441.
Kulabako, N.R., Nalubega, M., Thunvik, R., 2007. Study of the impact of land use and hydrogeological settings on the shallow groundwater quality in a peri-urban area of Kampala, Uganda. Sci. Total Environ. 381, 180–199. https://doi.org/10.1016/j.scitotenv.2007.03.035.
Kulabako, N.R., Nalubega, M., Thunvik, R., 2008. Phosphorus transport in shallow groundwater in peri-urban Kampala, Uganda: results from field and laboratory measurements. Environ. Geol. 53, 1535–1551. https://doi.org/10.1007/s00254-007-0764-0.
Langmuir, D., 1997. Aqueous Environmental Geochemistry. New Jersey.
Lapworth, D., Nkhuwa, D., Okotto-Okotto, J., Pedley, S., Stuart, M., Tijani, M., Wright, J., 2017. Urban groundwater quality in Sub-Saharan Africa: current status and implications for water security and public health. Hydrogeol. J. 25, 1093. https://doi.org/10.1007/s10040-016-1516-6.
Lapworth, D.J., MacDonald, A.M., Kebede, S., Owor, M., Chavula, G., Fallas, H., Wilson, P., Ward, J.S.T., Lark, M., Okullo, J., Cook, P., Casey, V., 2020. Drinking water quality from rural handpump-boreholes in Africa. Environ. Res. Lett. 15. https://doi.org/10.1088/1748-9326/ab8031.
Le Vaillant, M., Fiorentini, M.L., Barnes, S.J., 2016. Review of lithogeochemical exploration tools for komatiite-hosted Ni-Cu-(PGE) deposits. J. Geochem. Explor. 168, 1–19. https://doi.org/10.1016/j.gexplo.2016.05.010.
Leliveld, A., Dietz, T., Foeken, D., Klaver, W., Akinyoade, A., Smits, H., 2013. Agricultural dynamics and food security trends in Uganda. Dev. Regimes Afr. DRA Proj.
Luswata, K.C., Mbowa, S., 2015. Revisiting Uganda's Inorganic Fertilizer Supply Chain: Need for a Stronger Regulatory System. https://doi.org/10.22004/ag.econ.253561.
MAAIF, 2009. Uganda national rice development strategy. https://www.jica.go.jp/Resource/english/our_work/thematic_issues/agricultural/pdf/uganda_en.
MAAIF, 2016. NATIONAL FERTILISER POLICY. 10.22004/ag.econ, 257813.
Mackenzie, F.T., Garrels, R.M., 1965. Silicates: reactivity with sea water. Science 150, 57–58. https://doi.org/10.1126/science.150.3692.57.
Mackenzie, F.T., Garrels, R., 1971. Evolution of Sedimentary Rocks. Norton, New York.
Mayo, Alan L., Loucks, Mark D., 1995. Solute and isotopic geochemistry and ground water flow in the central Wasatch Range, Utah. J. Hydrol. 172 (1-4), 31–59. https://doi.org/10.1016/0022-1694(95)02748-e.
Miller, J., Miller, J.C., 2018. Statistics and Chemometrics for Analytical Chemistry. Pearson education.
Modenesi-Gauttieri, M.C., De Toledo, M.C.M., Hiruma, S.T., Taioli, F., Shimada, H., 2011. Deep weathering and landscape evolution in a tropical plateau. Catena 85, 221–230. https://doi.org/10.1016/j.catena.2011.01.006.
Muloogi, D., Wilson, G.J.L., Ahmed, F.T., Polya, D.A., Richards, L.A., 2025. Major groundwater chemistry of contrasting hydrogeological settings in Uganda. Presented at EGU General Assembly 2025. https://doi.org/10.5194/egusphere-egu25-662. EGU25-662).
Musumba, G., Sembatya, J., Muloogi, D., 2022. Temporal variations in physico-chemical parameters of ground water in Kibujjo village, Namayumba Sub-county, Wakiso district, Uganda. J. Water Resour. Protect. 14, 665–679. https://doi.org/10.4236/jwarp.2022.1410035.
Mwaura, F.M., Muwanika, F.R., 2018. Providing irrigation water as a public utility to enhance agricultural productivity in Uganda. Util. Policy 55, 99–109. https://doi.org/10.1016/j.jup.2018.09.003.
MWE, 2017. Consolidated Hydrological Year Book Uganda.
MWE, 2018. water-and-environment-strategic-investment-plan-2018-2030 (policy). Ministry Water Environ.
MWE, 2019. Water and environment sector performance report 2019. Ministry of water and environment. Minist. Water Environ. 279.
MWE, 2024. Water supply Atlas: national report. http://wsdb.mwe.go.ug/index.php/reports/national.
National Geographic Society, 2023. Nile river. Encycl. Entry Nile river. https://education.nationalgeographic.org/resource/nile-river/.
Njitchoua, R., Dever, L., Fontes, J.C., Naah, E., 1997. Geochemistry, origin and recharge mechanisms of groundwaters from the Garoua sandstone aquifer, northen Cameroon. J. Hydrol. 190, 123–140. https://doi.org/10.1016/S0022-1694(96)03049-1.
Nsubuga, F.N.W., Namutebi, E.N., Nsubuga-Ssenfuma, M., 2014. Water resources of Uganda: an assessment and review. J. Water Resour. Protect. 6, 1297–1315. https://doi.org/10.4236/jwarp.2014.6514120.
NWSC, 2023. National water and sewerage Corporation integrated annual report. https://www.nwsc.co.ug.
Nyakairu, G.W., Kasule, J., Ouma, O., Bahati, G., 2023. Origin and hydrogeochemical formation processes of geothermal fluids from the Kibiro area, Western Uganda. Appl. Geochem. 152, 105648. https://doi.org/10.1016/j.apgeochem.2023.105648.
Nyakairu, G.W., Kurzweil, H., Koeberl, C., 2002. Mineralogical, geochemical, and sedimentological characteristics of clay deposits from central Uganda and their applications. J. Afr. Earth Sci. 35, 123–134. https://doi.org/10.1016/S0899-5362(01)00077-X.
Nyenje, P.M., Foppen, J.W., Kulabako, R., Muwanga, A., Uhlenbrook, S., 2013. Nutrient pollution in shallow aquifers underlying pit latrines and domestic solid waste dumps in urban slums. J. Environ. Manag. 122, 15–24. https://doi.org/10.1016/j.jenvman.2013.02.040.
Nyenje, P.M., Foppen, J.W., Uhlenbrook, S., Lutterodt, G., 2014. Using hydrochemical tracers to assess impacts of unsewered urban catchments on hydrochemistry and nutrients in groundwater. Hydrol. Process. 28, 5860–5878. https://doi.org/10.1002/hyp.10070.
Nyenje, P.M., Ocoromac, D., Tumwesige, S., Ascott, M.J., Sorensen, J.P., Newell, A.J., Macdonald, D.M., Gooddy, D.C., Tindimugaya, C., Kulabako, R.N., 2022. Hydrogeology of an urban weathered basement aquifer in Kampala, Uganda. Hydrogeol. J. 30, 1469–1487. https://doi.org/10.1007/s10040-022-02474-9.
OCHA, 2020. Uganda - Subnational Administrative Boundaries. https://data.humdata.org/dataset/cod-ab-uga.
Ojok, W., Wanasolo, W., Wasswa, J., Bolender, J., Ntambi, E., 2021. Hydrochemistry and fluoride contamination in Ndali-Kasenda crater lakes, Albertine Graben: assessment

based on multivariate statistical approach and human health risk. Groundw. Sustain. Dev. 15. https://doi.org/10.1016/j.gsd.2021.100650.
Okot-Okumu, J., Otim, J., 2015. The quality of drinking water used by the communities in some regions of Uganda. Int. J. Biol. Chem. Sci. 9, 552. https://doi.org/10.4314/ijbcs.v9i1.47.
Oster, J., Sposito, G., Smith, C.J., 2016. Accounting for potassium and magnesium in irrigation water quality assessment. Calif. Agric. 70. https://doi.org/10.3733/ca.v070n02p71.
Owor, M., Muwanga, A., Tindimugaya, C., Taylor, R.G., 2021. Hydrogeochemical processes in groundwater in Uganda: a national-scale analysis. J. Afr. Earth Sci. 175, 104113. https://doi.org/10.1016/j.jafrearsci.2021.104113.
Owor, M., Okullo, J., Fallas, H., MacDonald, A.M., Taylor, R., MacAllister, D.J., 2022. Permeability of the weathered bedrock aquifers in Uganda: evidence from a large pumping-test dataset and its implications for rural water supply. Hydrogeol. J. 30, 2223–2235. https://doi.org/10.1007/s10040-022-02534-0.
Owor, M., Taylor, R., Mukwaya, C., Tindimugaya, C., 2011. Groundwater/surface-water interactions on deeply weathered surfaces of low relief: evidence from Lakes Victoria and Kyoga. Uganda. Hydrogeol. J. 19, 1403–1420. https://doi.org/10.1007/s10040-011-0779-1.
Owor, M., Tindimugaya, C., Brown, L., Upton, K., Dochartaigh, Ó., Bellwood-Howard, 2018. Africa Groundwater Atlas: Hydrogeology of Uganda. British Geological Survey.
Parkhurst, D.L., Appelo, C., 1999. User's guide to PHREEQC (Version 2): a computer program for speciation, batch-reaction, one-dimensional transport, and inverse geochemical calculations. US Geol. Survey. https://doi.org/10.3133/wri994259.
Pincetti-Zúniga, G.P., Richards, L.A., Tun, Y.M., Aung, H.P., Swar, A.K., Reh, U.P., Khaing, T., Hlaing, M.M., Myint, T.A., Nwe, M.L., Polya, D.A., 2020. Major and trace (including arsenic) groundwater chemistry in central and southern Myanmar. Appl. Geochem. 115, 104535. https://doi.org/10.1016/j.apgeochem.2020.104535.
Polya, D.A., Richards, L.A., Al Bualy, A.A.N., Sovann, C., Magnone, D., Lythgoe, P.R., 2017. Chapter A14. Best Pract. Guide 247.
Polya, D.A., Watts, M.J., 2017. Chapter 4: sampling and analysis for monitoring arsenic in drinking water. Best Pract. Guide Control Arsen. Drink. Water 49.
Rajesh, R., Brindha, K., Murugan, R., Elango, L., 2012. Influence of hydrogeochemical processes on temporal changes in groundwater quality in a part of Nalgonda district, Andhra Pradesh, India. Environ. Earth Sci. 65, 1203–1213. https://doi.org/10.1007/s12665-011-1368-2.
Ramsey, M.H., 1998. Sampling as a source of measurement uncertainty: techniques for quantification and comparison with analytical sources. J. Anal. At. Spectrom. 13, 97–104. https://doi.org/10.1039/A706815H.
Redwan, M., Abdel Moneim, A.A., 2016. Using Na/K ratios to identify the potential impacts of sewage effluent on groundwater quality in Sohag, Egypt. Groundw. Monit. Remediat. 36, 62–70. https://doi.org/10.1111/gwmr.12184.
Richards, L.A., Kumar, A., Shankar, P., Gaurav, A., Ghosh, A., Polya, D.A., 2020. Distribution and geochemical controls of arsenic and uranium in groundwater-derived drinking water in Bihar, India. Int. J. Environ. Res. Publ. Health 17, 2500. https://doi.org/10.3390/ijerph17072500.
Richards, L.A., Magnone, D., Sovann, C., Kong, C., Uhlemann, S., Kuras, O., van Dongen, B.E., Ballentine, C.J., Polya, D.A., 2017. High resolution profile of inorganic aqueous geochemistry and key redox zones in an arsenic bearing aquifer in Cambodia. Sci. Total Environ. 590–591, 540–553. https://doi.org/10.1016/j.scitotenv.2017.02.217.
Richards, L.A., Magnone, D., van Dongen, B.E., Ballentine, C.J., Polya, D.A., 2015. Use of lithium tracers to quantify drilling fluid contamination for groundwater monitoring in Southeast Asia. Appl. Geochem. 63, 190–202. https://doi.org/10.1016/j.apgeochem.2015.08.013.
Richards, L.A., Wilson, G., Wu, R., Muloogi, D., Hamisi, R., Denwood, T., Nuwategeka, E., Bhattacharya, P., Huck, J., Polya, D.A., 2023. Water quality in East Africa: bringing together traditional monitoring, community science and artificial intelligence approaches. Presented AGU Fall Meeting Abstracts H52C, 03.
Rodríguez-Iznaga, I., Shelyapina, M.G., Petranovskii, V., 2022. Ion exchange in natural clinoptilolite: aspects related to its structure and applications. Minerals 12, 1628. https://doi.org/10.3390/min12121628.
Rounds, S.A., 2012. Alkalinity and acid neutralizing capacity:U.S. geological survey techniques of water-resources investigations, book 9. Techniques of Water-Resources Investigations chap. 6.6 (No. 09-A6.6).
Rounds, S.A., Wilde, F.D., 2012. Chapter A6. Section 6.6. alkalinity and acid neutralizing capacity. US Geol. Survey.
Rusiniak, P., Sekuła, K., Sracek, O., Stopa, P., 2021. Fluoride ions in groundwater of the Turkana county, Kenya, East Africa. Acta Geochim. 40, 945–960. https://doi.org/10.1007/s11631-021-00481-3.
Schlüter, T., 2006. Uganda. Geol. Atlas Afr. Notes Stratigr. Tecton. Econ. Geol. 238–241. https://doi.org/10.1007/3-540-29145-8_3. Geohazards Geosites Each Ctry.
Schlüter, T., 2008. Geological Atlas of Africa. Springer. https://doi.org/10.1007/978-3-540-76373-4_1.
Schneider, S., Hornung, J., Hinderer, M., Garzanti, E., 2016. Petrography and geochemistry of modern river sediments in an equatorial environment (Rwenzori Mountains and albertine rift, Uganda)—implications for weathering and provenance. Sediment. Geol. 336, 106–119. https://doi.org/10.1016/j.sedgeo.2016.02.006.
Shand, P., Edmunds, W., Lawrence, A., Smedley, P., Burke, S., 2007. The Natural (Baseline) Quality of Groundwater in England and Wales. Environment Agency.
Shapiro, S.S., Wilk, M.B., 1965. An analysis of variance test for normality (complete samples). Biometrika 52, 591–611. https://doi.org/10.1093/biomet/52.3-4.591.
Tardy, Y., 1971. Characterization of the principal weathering types by the geochemistry of waters from some European and African crystalline massifs. Chem. Geol. 7, 253–271. https://doi.org/10.1016/0009-2541(71)90011-8.
Tay, C.K., 2012. Hydrochemistry of groundwater in the savelugu–Nanton district, northern Ghana. Environ. Earth Sci. 67, 2077–2087. https://doi.org/10.1007/s12665-012-1647-6.
Taylor, R.G., Howard, K.W.F., 1995. Groundwater quality in rural Uganda: hydrochemical considerations for the development of aquifers within the basement complex of Africa. In: Groundwater Quality. Chapman and Hall, London, pp. 31–44.
Taylor, R., Howard, K., 2000. A tectono-geomorphic model of the hydrogeology of deeply weathered crystalline rock: evidence from Uganda. Hydrogeol. J. 8, 279–294. https://doi.org/10.1007/s100400000069.
Tindimugaya, C., 2005. Groundwater Resources Management in Urban Areas of Uganda: Experiences and Challenges. Loughborough University. Conference contribution. https://hdl.handle.net/2134/29225.
UBOS, 2024. National population and housing census. https://www.ubos.org.
UNICEF Uganda, 2024. U-Report: amplifying voices for young people. https://www.unicef.org/uganda.
United Nations, 2023. Independent Group of Scientists Appointed by the Secretary-General, Global Sustainable Development Reprt 2023: times of Crisis, Times of Change: Science for Accelerating Transformations to Sustainable Development. Global Sustainability Report, New York. https://sdgs.un.org.
UNMA, 2023. Uganda National Meterological Survey Outlook. http://www.meteo.mwe.go.ug.
USSL, 1954. Diagnosis and Improvement of Saline and Alkaline Soils, No. 60. US Department of Agriculture, Handbook. https://www.ars.usda.gov.
Uzorka, A., Candia, J., Ouyesiga, L., Olaniyan, A.O., 2025. Radiological health risk assessment of borehole water in Arua city, Northern Uganda. Water Res., 124690 https://doi.org/10.1016/j.watres.2025.124690.
Walraevens, K., Bakundukize, C., Mtoni, Y.E., Van Camp, M., 2018. Understanding the hydrogeochemical evolution of groundwater in Precambrian basement aquifers: a case study of Bugesera region in Burundi. J. Geochem. Explor. 188, 24–42. https://doi.org/10.1016/j.gexplo.2018.01.003.
Wangi, G.M., Olupot, P.W., Byaruhanga, J., Kulabako, R., 2023. Characterization of natural zeolite and determination of its ion-exchange potential for selected metal ions in water. Environ. Process. 10. https://doi.org/10.1007/s40710-023-00654-7.
Ward Jr, J.H., 1963. Hierarchical grouping to optimize an objective function. J. Am. Stat. Assoc. 58, 236–244. https://doi.org/10.1080/01621459.1963.10500845.
Westerhof, A.B., Härmä, P., Isabirye, E., Katto, E., Koistinen, T., Kuosmanen, E., Lehto, T., Lehtonen, M., Mäkitie, H., Manninnen, T., Mänttäri, I., Pekkala, Y., Pokki, J., Saalmann, K., Virransalo, P., 2014. Geology and Geodynamic Development of Uganda with Explanation of the 1:1,000,000 Scale Geological Map. Geological Survey of Finland. Special Paper 55.
WHO, 2017. 2017 WHO guidelines for drinking water quality: first addendum to the fourth edition. J.-Am. Water Works Assoc. 109, 44–51. https://doi.org/10.5942/jawwa.2017.109.0087.
Williams, L., 1969. Volcanic associations in the Gregory rift valley, East Africa. Nature 224, 61–64. https://doi.org/10.1038/224061a0.
Wilson, G.J., Hamisi, R., Denwood, T., Muloogi, D., Bhattacharya, P., Nuwategeka, E., Gooddy, D.C., Polya, D.A., Huck, J.J., Richards, L.A., 2024b. Geochemical tracers reveal urban-derived contamination of groundwater and springs in Gulu city, Uganda. Copernicus Meet. https://doi.org/10.5194/egusphere-egu24-9232.
Wilson, G.J., Muloogi, D., Hamisi, R., Denwood, T., Bhattacharya, P., Nuwategeka, E., Gooddy, D.C., Polya, D.A., Huck, J.J., Richards, L.A., 2024a. Surface-derived groundwater contamination in Gulu district, Uganda: chemical and microbial tracers. Sci. Total Environ., 177118 https://doi.org/10.1016/j.scitotenv.2024.177118.
Xu, F., Li, P., 2024. Biogeochemical mechanisms of iron (Fe) and manganese (Mn) in groundwater and soil profiles in the zhongning section of the Weining plain (northwest China). Sci. Total Environ., 173506 https://doi.org/10.1016/j.scitotenv.2024.173506.
Zaidi, F.K., Nazzal, Y., Jafri, M.K., Naeem, M., Ahmed, I., 2015. Reverse ion exchange as a major process controlling the groundwater chemistry in an arid environment: a case study from northwestern Saudi Arabia. Environ. Monit. Assess. 187, 1–18. https://doi.org/10.1007/s12665-015-4120-5.
Zhai, Y., Cao, X., Xia, X., Wang, B., Teng, Y., Li, X., 2021. Elevated Fe and Mn concentrations in groundwater in the Songnen plain, Northeast China, and the factors and mechanisms involved. Agronomy 11, 2392. https://doi.org/10.3390/agronomy11122392.